IOP Publishing Physica Scripta
Phys. Scr. 95 (2020) 055004 (17pp) https://doi.org/10.1088/1402-4896/ab6f94

Deformation analysis of a viscoelastic half-space due to a finite and an infinite interacting faults

Piu Kundu[1] **and Seema Sarkar (Mondal)**

Department of Mathematics, National Institute of Technology Durgapur, Durgapur-713209, India

E-mail: piukundu91@gmail.com and seemasarkarmondal17@gmail.com

Received 1 October 2019, revised 23 January 2020
Accepted for publication 24 January 2020
Published 3 March 2020

Abstract

In seismically active regions the process of stress–strain accumulation near earthquake faults during aseismic period (period in between two major seismic events) has become a subject of research during the last few decades. The occurrence of multiple faults (for example Calaveras, Garlock in the neighbourhood of San Andreas fault) in seismically active region is more likely than that of a single fault (i.e. Sierra Madre fault, Raymond fault). Moreover the earthquake faults involve both the strike-slip and dip-slip faults some of which may be finite and others infinite. The way of interaction of faults with each other controls fault geometries, displacements and strains. Such phenomena encourage us to consider a model of interacting strike-slip and dip-slip faults in which a finite and an infinite interacting faults are taken to study the stress–strain accumulation in the neighbouring fault due to the movement across the other fault. The solutions for displacement, stress and strain are then found before the onset of fault slip and then superpose the effect of fault slip for both the interacting faults using Laplace transform, suitable mathematical technique of modified Green's function and Correspondence principal. The analytical results and the graphical presentations show that the velocities of both the faults movement and their inclinations have noticeable effects on displacements, stresses and strains.

Keywords: infinite and finite strike-slip fault, infinite strike-slip and finite dip-slip fault, creeping fault, aseismic period, Green's function technique

(Some figures may appear in colour only in the online journal)

1. Introduction

Active fault system in seismically active regions often consists of multiple faults some of which are interacting faults having different inclinations with the horizontal. Faults like Calaveras, Garlock, Hayward, San Jacinto etc. are neighbouring and interacting faults which are found in the western part of North America near San Andreas fault. In such neighbouring faults, movement across any one will have a significant effect on the accumulation of stress and strain near the others and thereby affect the possibilities of movement across them. There are some dynamic models of fault systems which consists of two interacting strike-slip faults and some other models in which combination of strike-slip and dip-slip faults are found. Some theoretical models of the lithosphere-asthenosphere system in seismically active regions during aseismic periods with two interacting creeping/slipping faults have been developed by Mukhopadhyay *et al* (1978b [1], 1979c [2]), Mukhopadhya and Mukherji (1984 [3], 1986 [4]) Ghosh *et al* (1992a [5], 1992b [6]) and Ghosh and Sen (2011 [7]). Kato and Lei (2001 [8]) demonstrated a numerical simulation of the activities of many parallel strike-slip faults embedded in an elastic layer over a viscoelastic half-space. Bonafede *et al* (1984 [9]) developed a model for two parallel strike-slip faults to investigate interactions between them. A model has been described by Debnath and Sen (2014 [10]) about the interaction between two neighbouring infinite strike-slip faults in standard linear solids. Wesnousky (1988 [11])

[1] Author to whom any correspondence should be addressed.

cited many earthquakes on major strike-slip faults that both were bounded by and ruptured through compressional and dilational step-overs. In analyzing the seismic hazard of the San Francisco Bay region, Parsons *et al* (2003 [12]) studied the potential interaction of the Hayward and Rodgers Creek faults at the extensional step-over that separates the two faults underneath San Pablo Bay. One of the important issues that they addressed is whether a normal fault exists in the step-over region, under such assumption that such linking normal faults could increase the probability of rupture propagating across the step-over. Oglesby (2005[13]) developed a model of the dynamics of fault systems consisting of strike-slip fault step-over linked by dip-slip faults. Harris and Day (1993 [14]) analyzed two-dimensional dynamic models of stepovers in strike-slip faults to consider their interaction. Segall and Pollard (1980 [15]) did include fault interaction in their two-dimensional quasi-static study of strike-slip faults. Mavko (1982 [16]) also modelled fault interaction using two dimensional quasi-static calculations. He used his results to successfully explain the creep records on the San Andreas fault near Hollister, California. Shao and Guiting (2019 [17]) have discussed the interactions of fault patterns and stress fields during active faulting in Central North China Block by using numerical simulation. Attanayake *et al* (2019 [18]) have explained about interacting intraplate Fault Systems in Australia.

Debnath (2013 [19]) have described a model of two interacting creeping vertical finite strike-slip faults in a visco-elastic half-space of the lithosphere. A model of interaction between two long inclined strike-slip faults in layered medium has been described by Manna and Sen (2017 [20]). The fault system can comprise of both the infinite (i.e. long) and finite faults. For example San Andreas fault in California is infinite strike-slip fault and in the neighbouring of this fault Calaveras, Hyward, san Jacinto are finite strike-slip fault. To the best of our knowledge no theoretical models involving interaction between an infinite and finite strike-slip fault have still been developed. The fault system may involve not only set of finite faults or set of infinite faults, but it may also involve set which is combination of finite and infinite faults some of which may be strike-slip and the others may be dip-slip in nature. Hence fault movement ether across an infinite strike-slip or across interacting faults of the nature of strike-slip and dip-slip may have effect on displacement, stress and strain of the other. Hence for elaborate study, a model of interacting strike-slip faults—one infinite and other finite—in viscoelastic half-space of Maxwell medium has been considered in this paper. The variation of displacement, stress and strain components have been studied analytically. Also a model of interaction between an infinite strike-slip and a finite dip-slip fault is studied. The objective of these studies is to observed the effect of movement of one fault on displacement, stress and strain of the other during the following three situations for different inclinations of the faults and different velocities of their movement; (i) when there is no fault movement across any fault (ii) when there is movement across infinite fault but no movement across finite fault and (iii) when the movement occurs across both the faults.

A fault is said to be an infinite fault if its length is large enough compared to its width, otherwise the fault is said to be finite. The line of the intersection of the fault plane with the free surface of the Earth is known as the strike direction while a line in the fault plane perpendicular to the strike in the downwards direction is the dip of the fault. The characteristic of the fault is determined according to the relative motion across it. If this relative motion is predominantly parallel to the fault strike is called strike-slip fault, whereas if the motion is predominantly parallel to the fault dip is called dip-slip fault.

The rest of the paper is organised as follows: In section 2, description of the model and the formulation of the problem with constitutive equations, stress equations of motion, boundary conditions and initial conditions has been discussed. The solution of displacements, stresses and strains have been analyzed and some numerical computations have been carried out in section 3. Further in section 4, the results have been discussed. Finally the paper ends with a conclusion and future scope of our work as given in section 5.

2. Formulation

Two interacting faults F_1 and F_2 have been shown in figure 1 where F_1 is infinite and F_2 is finite. To study the effect of the fault movement two cases have been considered that is case-I for both F_1 and F_2 are strike-slip and case-II for F_1 strike-slip but F_2 dip-slip.

Case-I:

The interacting strike-slip faults F_1 and F_2 are inclined to the horizontal at an angle θ_1 and θ_2 respectively and both buried in a visco-elastic half-space of Maxwell medium (figure 1) where F_1 is infinite and F_2 is finite of length 2L (L —finite).

Let D_1 and D_2 be the respective widths of the faults F_1 and F_2 with d_1 and d_2 as their corresponding depth and D be the distance between them on the free surface.

Two sets of rectangular cartesian co-ordinate system (y_1, y_2, y_3) and (y_1', y_2', y_3') have been chosen as for F_1 and two other sets (z_1, z_2, z_3) and (y_1'', y_2'', y_3'') for F_2 as described in figure 1. y_3 and z_3 axes are pointing into the half-space with $y_3 = 0$ and $z_3 = 0$ as free surface. y_1 and z_1 axes are vertically above the upper edges of the faults. These systems are associated by the following relations:

$$\left.\begin{aligned} y_1' &= y_1 \\ y_2' &= y_2 \sin\theta_1 - (y_3 - d_1)\cos\theta_1 \\ y_3' &= y_2 \cos\theta_1 + (y_3 - d_1)\sin\theta_1 \end{aligned}\right\} \tag{1}$$

and

$$\left.\begin{aligned} y_1'' &= z_1 \\ y_2'' &= z_2 \sin\theta_2 - z_3 \cos\theta_2 \\ y_3'' &= z_2 \cos\theta_2 + z_3 \sin\theta_2 \end{aligned}\right\}, \tag{2}$$

where $z_2 = y_2 - D$ and $z_3 = y_3 - d_2$

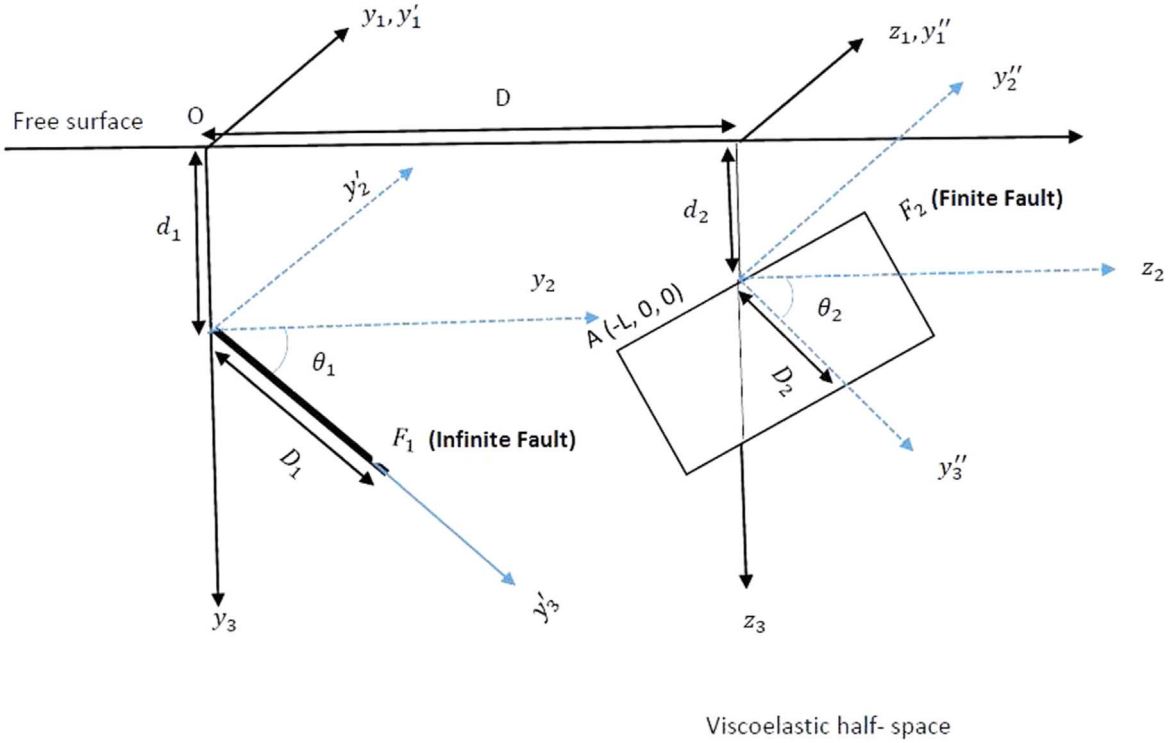

Figure 1. Two interacting buried strike-slip faults: one infinite and other finite.

Thus faults F_1 and F_2 are given by F_1: $(y_2' = 0,\ 0 \leqslant y_3' \leqslant D_1)$ and F_2: $(-L \leqslant y_1'' \leqslant L,\ y_2'' = 0,\ 0 \leqslant y_3'' \leqslant D_2)$

Here we assume that the length of the fault F_1 is large compared to its width, so that the displacements, stresses and strains are independent of y_1 and depend on y_2, y_3 and t. Since F_2 is finite, the displacements, stresses and strains are function of y_1, y_2, y_3 and t.

2.1. Constitutive equations

The constitutive equations relate the stresses acting on a materiel element to the resultant strains and/or rates of strain.

Since for the infinite strike-slip fault, displacement, stress and strain components are independent of y_1, these components associate with F_1 fault are u_1, τ_{13} (stress act on the plane perpendicular to y_1 axis and in y_3 direction), τ_{12} ((stress act on the plane perpendicular to y_1 axis and in y_2 direction), e_{13} (strain on the plane perpendicular to y_1 axis and in y_3 direction) and e_{12} (strain on the plane perpendicular to y_1 axis and in y_2 direction).

For a visco-elastic medium of Maxwell type, the constitutive equations have been taken as for infinite fault F_1:

$$\left.\begin{aligned}\left(\frac{1}{\eta}+\frac{1}{\mu}\frac{\partial}{\partial t}\right)\tau_{12} &= \frac{1}{2}\frac{\partial}{\partial t}\left(\frac{\partial u_1}{\partial y_2}+\frac{\partial u_2}{\partial y_1}\right)\\ \left(\frac{1}{\eta}+\frac{1}{\mu}\frac{\partial}{\partial t}\right)\tau_{13} &= \frac{1}{2}\frac{\partial}{\partial t}\left(\frac{\partial u_1}{\partial y_3}+\frac{\partial u_3}{\partial y_1}\right)\end{aligned}\right\} \tag{3}$$

and for finite fault F_2:

$$\left.\begin{aligned}\left(\frac{1}{\eta}+\frac{1}{\mu}\frac{\partial}{\partial t}\right)\tau_{11} &= \frac{\partial}{\partial t}\left(\frac{\partial u_1}{\partial y_1}\right)\\ \left(\frac{1}{\eta}+\frac{1}{\mu}\frac{\partial}{\partial t}\right)\tau_{12} &= \frac{1}{2}\frac{\partial}{\partial t}\left(\frac{\partial u_1}{\partial y_2}+\frac{\partial u_2}{\partial y_1}\right)\\ \left(\frac{1}{\eta}+\frac{1}{\mu}\frac{\partial}{\partial t}\right)\tau_{13} &= \frac{1}{2}\frac{\partial}{\partial t}\left(\frac{\partial u_1}{\partial y_3}+\frac{\partial u_3}{\partial y_1}\right)\\ \left(\frac{1}{\eta}+\frac{1}{\mu}\frac{\partial}{\partial t}\right)\tau_{22} &= \frac{\partial}{\partial t}\left(\frac{\partial u_2}{\partial y_2}\right)\\ \left(\frac{1}{\eta}+\frac{1}{\mu}\frac{\partial}{\partial t}\right)\tau_{23} &= \frac{1}{2}\frac{\partial}{\partial t}\left(\frac{\partial u_2}{\partial y_3}+\frac{\partial u_3}{\partial y_2}\right)\\ \left(\frac{1}{\eta}+\frac{1}{\mu}\frac{\partial}{\partial t}\right)\tau_{33} &= \frac{\partial}{\partial t}\left(\frac{\partial u_3}{\partial y_3}\right)\end{aligned}\right\}, \tag{4}$$

where η is effective viscosity and μ is shear modulus.

2.2. Stress equation of motion

The stresses satisfy the following equations by assuming quasi-static deformations for which the inertial terms are neglected and body forces do not change during our consideration.

For infinite fault F_1

$$\left.\frac{\partial}{\partial y_2}(\tau_{12})+\frac{\partial}{\partial y_3}(\tau_{13})=0\right\} \tag{5}$$

and for finite fault F_2

$$\left.\begin{aligned}\frac{\partial}{\partial y_1}(\tau_{11})+\frac{\partial}{\partial y_2}(\tau_{12})+\frac{\partial}{\partial y_3}(\tau_{13})=0\\ \frac{\partial}{\partial y_1}(\tau_{21})+\frac{\partial}{\partial y_2}(\tau_{22})+\frac{\partial}{\partial y_3}(\tau_{23})=0\\ \frac{\partial}{\partial y_1}(\tau_{31})+\frac{\partial}{\partial y_2}(\tau_{32})+\frac{\partial}{\partial y_3}(\tau_{33})=0\end{aligned}\right\}. \tag{6}$$

2.3. Boundary conditions

The boundary conditions are taken as with $t = 0$, representing an instant when the medium is in aseismic state. The infinite fault F_1 moves after time $t = T_1(>0)$ and finite fault F_2 moves after time $t = T_2$, where $T_1 < T_2$.

Since for the fault F_1 the stress components only act on the plane perpendicular to y_1 axis and in y_2 and y_3 direction, then the boundary conditions will be as follows:

On the free surface i.e. on $y_3 = 0$,

$$\tau_{13} = 0 \ \ (-\infty < y_2 < \infty, \ t \geqslant 0) \tag{7}$$

$$\text{As } y_3 \to \infty, \ \tau_{13} \to 0 \ \ (-\infty < y_2 < \infty, \ t \geqslant 0), \tag{8}$$

$$\tau_{12} \to \tau_\infty(t) \ \text{ as } |y_2| \to \infty \ (y_3 \geqslant 0, \ t \geqslant 0), \tag{9}$$

where τ_{12} is the main driving force for strike-slip fault and $\tau_\infty(t)$ is the value of τ_{12} far away from the fault maintained by tectonic forces. It may or may not change with time, but it is independent of y_3. If it changes with time

$\tau_\infty(t) = \tau_\infty(0)(1 + kt)$ (say), where $k \geqslant 0$ is a constant. Then

$$\tau_{12} \to \tau_\infty(t) = \tau_\infty(0)(1 + kt), \quad k > 0, \ \text{as } |y_2| \to \infty \text{ for } y_3 \geqslant 0, \ t \geqslant 0 \tag{10}$$

$\tau_\infty(0)$ = the value of $\tau_\infty(t)$ at $t = 0$

$\tau_{12}(0) \to \tau_\infty(0)$ as $|y_2| \to \infty$ for $t = 0$.

2.4. Initial conditions

The time t is measured from a suitable instant when the model is in aseismic state and no seismic disturbance occurs. Let $(u_i)_0$, $(\tau_{ij})_0$ and $(e_{ij})_0$ are the value of u_i, τ_{ij} and e_{ij} at $t = 0$.

3. Solution

Now differentiating the first and second equation of (3) w.r.t y_2 and y_3 respectively, then adding and finally using equation (5) we get

$$\nabla^2 u_1 = 0 \text{ (detail in APPENDIX).} \tag{11}$$

The displacement satisfy Laplace's equation and this is a general solution.

3.1. Displacement, stress and strain in the absence of fault movement

The displacement, stress, and strain components are continuous throughout the system. All the constitutive equations and boundary conditions (3)–(10) are valid. Laplace Transform of all the constitutive equations and boundary conditions results in the boundary value problem which can be solved (detail in appendix). By taking inverse Laplace transform, the solutions for displacements, stresses and strains are obtained in the absence of fault movement (for $t < T_1$) as follows:

$$\left.\begin{aligned}u_1 &= (u_1)_0 + \tau_\infty(t)\left[\left(\frac{1}{\eta}+\frac{k}{\mu}\right)t+\frac{kt^2}{2\eta}\right]y_2\\ u_2 &= 0\\ u_3 &= 0\\ \tau_{11} &= 0\\ \tau_{12} &= (\tau_{12})_0\, e^{\left(-\frac{\mu t}{\eta}\right)} + \tau_\infty(0)[1-e^{-\frac{\mu t}{\eta}}+kt]\\ \tau_{13} &= (\tau_{13})_0\, e^{\left(-\frac{\mu t}{\eta}\right)}\\ \tau_{22} &= 0\\ \tau_{23} &= 0\\ \tau_{33} &= 0\\ e_{12} &= (e_{12})_0 + \frac{\tau_\infty(t)}{2}\left[t\left(\frac{1}{\eta}+\frac{k}{\mu}\right)+\frac{kt^2}{2\eta}\right]\\ e_{13} &= (e_{13})_0\end{aligned}\right\}. \tag{12}$$

Now, τ'_{12} = Stress component which tends to cause strike-slip movement across the fault $F_1 = \tau_{12}\sin\theta_1 - \tau_{13}\cos\theta_1 = (\tau'_{12})_0\, e^{\left(-\frac{\mu t}{\eta}\right)} + \tau_\infty(0)\,[1 - e^{-\frac{\mu t}{\eta}} + kt]\,\sin\theta_1$. where $(\tau'_{12})_0 = (\tau_{12})_0\sin\theta_1 - (\tau_{13})_0\cos\theta_1$.

It is observed that for the fault F_1 the relevant stress component τ'_{12} increases with time and finally tends to $\tau_\infty \sin\theta_1$. The fault F_1 starts to slip when the magnitude of stress τ'_{12} reaches a threshold value say τ_{c_1} ($<\tau_\infty \sin\theta_1$) after a time T_1.

3.2. Displacement, stress and strain components after the commencement of fault movement

We assume that the movement of the fault F_1 occurs at time $t = T_1(>0)$ while the other fault F_2 remains locked. The equations (3), (5), (7)–(10) remain valid for $t \geqslant T_1$. But in addition we have the following condition which characterizes the slip across F_1:

$$[u_1]_{F_1} = U_1(t_1)\, f(y'_3)\, H(t_1) \times (y'_2 = 0, \ 0 \leqslant y'_3 \leqslant D_1, \ t_1 \geqslant 0, \ t_1 = t - T_1), \tag{13}$$

where $[u_1]_{F_1}$ is the relative displacement across F_1 and the discontinuity of displacement u_1 is given by

$$[u_1]_{F_1} = \lim_{(y'_2 \to 0^+)}(u_1) - \lim_{(y'_2 \to 0^-)}(u_1) \tag{14}$$

$H(t_1)$ is the Heaviside function, $f(y'_3)$ is a continuous function which gives the spatial dependence of the slip movement along the fault F_1 and $U_1(t_1) = v_1 t_1$, v_1 is the velocity of the fault movement across F_1.

Taking Laplace transform on equation (13) gives

$[\bar{u_1}]_{F_1} = U_1(p)\, f(y'_3)$, where $\bar{u_1}$ represents Laplace transform of u_1.

The fault creep commences across F_1 after time T_1.

Clearly $[(u_1)]_{F_1} = 0$ for $t_1 \leqslant 0$, where $t_1 = t - T_1$.

Let us first consider the slip across the fault F_1 after a time T_1. Due to movement across the fault F_1, the near region of F_1 becomes distributed and hence the constitutive equations do not remain valid and this short duration of time leave out. However, the disturbances gradually die out with time and an aseismic state re-established. This model have re-considered after the restoration of this aseismic state in the region. Then the solution of displacements, stresses and strains after the commencement of fault movement across F_1 can be obtained in the following form:

$$\left.\begin{aligned} u_1 &= (u_1)_1 + (u_1)_2 \\ u_2 &= (u_2)_1 + (u_2)_2 \\ u_3 &= (u_3)_1 + (u_3)_2 \\ \tau_{11} &= (\tau_{11})_1 + (\tau_{11})_2 \\ \tau_{12} &= (\tau_{12})_1 + (\tau_{12})_2 \\ \tau_{13} &= (\tau_{13})_1 + (\tau_{13})_2 \\ \tau_{23} &= (\tau_{23})_1 + (\tau_{23})_2 \\ \tau_{22} &= (\tau_{22})_1 + (\tau_{22})_2 \\ \tau_{33} &= (\tau_{33})_1 + (\tau_{33})_2 \\ e_{12} &= (e_{12})_1 + (e_{12})_2 \\ e_{13} &= (e_{13})_1 + (e_{13})_2 \end{aligned}\right\} \tag{15}$$

where $(u_i)_1$ $(i = 1,\ 2,\ 3)$, $(\tau_{ij})_1$, and $(e_{ij})_1$ $(i,\ j = 1,\ 2,\ 3)$ are given in equation (12). $(u_i)_2$ $(i = 1,\ 2,\ 3)$, $(\tau_{ij})_2$, and $(e_{ij})_2$ $(i,\ j = 1,\ 2,\ 3)$ satisfy the conditions (3), (5), (7)–(10). They are obtained by using modified form of Green's function technique developed by Maruyama [21, 22] and Rybicki [23, 24] as explained in appendix. Since the fault F_1 is infinite and strike slip, the components $(u_2)_2$, $(u_3)_2$, $(\tau_{11})_2$, $(\tau_{23})_2$, $(\tau_{22})_2$, $(\tau_{33})_2$ are all equal to zero and $(u_1)_2$ satisfy the dislocation condition (14).

We get

$$\left.\begin{aligned} (u_1)_2 &= \frac{U(t_1)}{2\pi} H(t_1)\,\psi(y_2,\ y_3) \\ (\tau_{12})_2 &= \frac{H(t_1)}{2\pi}\mu\,[U_1(t_1) - \frac{\mu}{\eta}\int_0^{t_1} U_1(\tau)\mathrm{e}^{-\frac{\mu}{\eta}(t_1-\tau)}\mathrm{d}\tau]\,\psi_2(y_2,\ y_3) \\ (\tau_{13})_2 &= \frac{H(t_1)}{2\pi}\mu\,[U_1(t_1) - \frac{\mu}{\eta}\int_0^{t_1} U_1(\tau)\mathrm{e}^{-\frac{\mu}{\eta}(t_1-\tau)}\mathrm{d}\tau]\,\psi_3(y_2,\ y_3) \\ (e_{12})_2 &= H(t_1)\frac{U_1(t_1)}{4\pi}\psi_2(y_2,\ y_3) \\ (e_{13})_2 &= H(t_1)\frac{U_1(t_1)}{4\pi}\psi_3(y_2,\ y_3) \end{aligned}\right\}, \tag{16}$$

where ψ is given in appendix and $\psi_2 = \frac{\partial\psi}{\partial y_2}$, $\psi_3 = \frac{\partial\psi}{\partial y_3}$.

From these solutions that the stress accumulation or release has been found due to movement across the fault F_1.

Next It is assumed that the finite fault F_2 slips after time T_2 $(T_2 > T_1)$ when the accumulated stress near it exceeds the critical value τ_{c_2}(say).

The slip condition is characterized by:

$$[u_1]_{F_2} = U_2(t_2)\,f(y''_1,\ y''_3)\,H(t_2) \tag{17}$$

$(-L \leqslant y''_1 \leqslant L,\quad y''_2 = 0,\ 0 \leqslant y''_3 \leqslant D_2),\quad t_2 \geqslant 0,\quad t_2 = t - T_2)$

$[u_1]_{F_2}$ is the relative displacement across F_2 given by

$$[u_1]_{F_2} = \lim_{(y''_2 \to 0^+)} (u_1) - \lim_{(y''_2 \to 0^-)} (u_1) \tag{18}$$

$H(t_2)$ is the Heaviside function, $f(y''_1,\ y''_3)$ gives the spatial dependence of the slip movement along the fault F_2 and $U_2(t_2) = v_2 t_2$, v_2 is the velocity of the fault movement across F_2.

Laplace transform on equation (17) gives

$[\bar{u_1}]_{F_2} = U_2(p)\,f(y''_1,\ y''_3)$, where $U_2(p)$ is Laplace transform of $U_2(t_2)$.

Since the fault creep commences across F_2 after time T_2 hence $[(u_1)]_{F_2} = 0$ for $t_2 \leqslant 0$, where $t_2 = t - T_2$.

Then final solution for displacements, stresses and strains after the movement across both the faults F_1 and F_2 are given by

$$\left.\begin{aligned} u_i &= (u_i)_1 + (u_i)_2 + (u_i)_3\ (i = 1,\ 2,\ 3) \\ \tau_{ij} &= (\tau_{ij})_1 + (\tau_{ij})_2 + (\tau_{ij})_3,\ (i,\ j = 1,\ 2,\ 3) \\ e_{12} &= (e_{12})_1 + (e_{12})_2 + (e_{12})_3 \\ e_{13} &= (e_{13})_1 + (e_{13})_2 + (e_{13})_3 \end{aligned}\right\}, \tag{19}$$

where $(u_i)_1$ $(i = 1,\ 2,\ 3)$, $(\tau_{ij})_1$ $(i,\ j = 1,\ 2,\ 3)$, $(e_{12})_1$, $(e_{13})_1$ are taken from equations (12) and $(u_i)_2$ $(i = 1,\ 2,\ 3)$, $(\tau_{ij})_2$ $(i,\ j = 1,\ 2,\ 3)$, $(e_{12})_2$, $(e_{13})_2$ are from equation (16). It has found that the values of $(u_i)_3$ $(i = 1,\ 2,\ 3)$, $(\tau_{ij})_3$ $(i,\ j = 1,\ 2,\ 3)$, $(e_{12})_3$ and $(e_{13})_3$ depending on the fault slip across F_2. $(u_i)_3$ $(i = 1,\ 2,\ 3)$, $(\tau_{ij})_3$ $(i,\ j = 1,\ 2,\ 3)$, $(e_{12})_3$, $(e_{13})_3$ satisfy equation (4), (6)–(10) and their values are assumed to be zero for $t \leqslant T_2$.

So we get

$$\left.\begin{aligned} (u_1)_3 &= \tfrac{U_2(t_2)}{2\pi}\phi(z_1,\ z_2,\ z_3)H(t_2) \\ (u_2)_3 &= 0 \\ (u_3)_3 &= 0 \\ (\tau_{11})_3 &= \tfrac{H(t_2)}{2\pi}\mu\,[U_2(t_2) - \tfrac{\mu}{\eta}\int_0^{t_2} U_2(\tau)\mathrm{e}^{-\frac{\mu}{\eta}(t_2-\tau)}\mathrm{d}\tau]\,\phi_1(z_1,\ z_2,\ z_3) \\ (\tau_{12})_3 &= \tfrac{H(t_2)}{2\pi}\mu\,[U_2(t_2) - \tfrac{\mu}{\eta}\int_0^{t_2} U_2\tau\mathrm{e}^{-\frac{\mu}{\eta}(t_2-\tau)}\mathrm{d}\tau]\,\phi_2(z_1,\ z_2,\ z_3) \\ (\tau_{13})_3 &= \tfrac{H(t_2)}{2\pi}\mu\,[U_2(t_2) - \tfrac{\mu}{\eta}\int_0^{t_2} U_2\tau\mathrm{e}^{-\frac{\mu}{\eta}(t_2-\tau)}\mathrm{d}\tau]\,\phi_3(z_1,\ z_2,\ z_3) \\ (\tau_{22})_3 &= \mathrm{e}^{-\frac{\mu}{\eta}t_2}(\tau_{22})_0 \\ (\tau_{23})_3 &= \mathrm{e}^{-\frac{\mu}{\eta}t_2}(\tau_{23})_0 \\ (\tau_{33})_3 &= \mathrm{e}^{-\frac{\mu}{\eta}t_2}(\tau_{33})_0 \\ (e_{12})_3 &= \tfrac{U_2(t_2)}{4\pi}H(t_2)\phi_2(z_1,\ z_2,\ z_3) \\ (e_{13})_3 &= \tfrac{U_2(t_2)}{4\pi}H(t_2)\phi_3(z_1,\ z_2,\ z_3) \end{aligned}\right\}, \tag{20}$$

where ϕ given in appendix and $\phi_1 = \frac{\partial\phi}{\partial y_1}$, $\phi_2 = \frac{\partial\phi}{\partial y_2}$, $\phi_3 = \frac{\partial\phi}{\partial y_3}$.

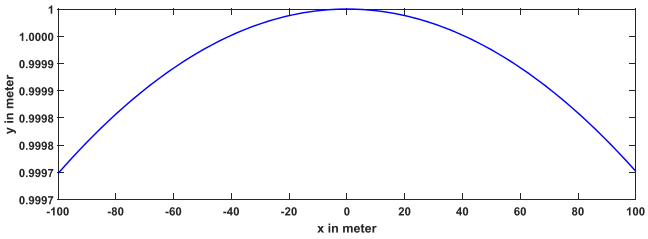

Figure 2. Creep function for F_1 fault.

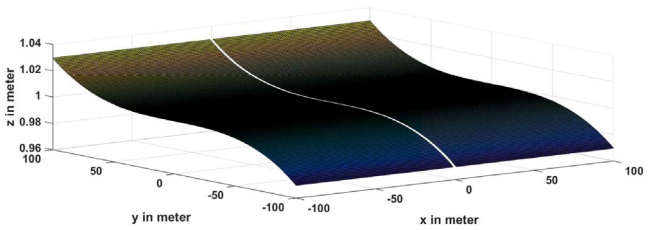

Figure 3. Creep function for F_2 fault.

Finally the complete solutions for displacement, stress and strain after both F_1 and F_2 fault movement are obtained as follows:

$$\left.\begin{aligned}
&u_1 = (u_1)_0 + \tau_\infty(0)[(\tfrac{1}{\eta} + \tfrac{k}{\mu})t + \tfrac{kt^2}{2\eta}]y_2 + \tfrac{U_1(t_1)}{2\pi}\psi(y_2, y_3)H(t_1) + \tfrac{U_2(t_2)}{2\pi}\phi(z_1, z_2, z_3)H(t_2)\\
&u_2 = 0\\
&u_3 = 0\\
&\tau_{11} = \tfrac{H(t_2)}{2\pi}\mu\,[U_2(t_2) - \tfrac{\mu}{\eta}\int_0^{t_2} U_2(\tau)e^{-\frac{\mu}{\eta}(t_2-\tau)}\mathrm{d}\tau]\,\phi_1\\
&\tau_{12} = (\tau_{12})_0\,\mathrm{e}^{-\frac{\mu}{\eta}t} + \tau_\infty(0)[1-\mathrm{e}^{-\frac{\mu t}{\eta}} + kt] + \tfrac{H(t_1)}{2\pi}\mu\,[U_1(t_1) - \tfrac{\mu}{\eta}\int_0^{t_1} U_1(\tau)\mathrm{e}^{-\frac{\mu}{\eta}(t_1-\tau)}\mathrm{d}\tau]\,\psi_2\\
&\qquad + \tfrac{H(t_2)}{2\pi}\mu\,[U_2(t_2) - \tfrac{\mu}{\eta}\int_0^{t_2} U_2(\tau)\mathrm{e}^{-\frac{\mu}{\eta}(t_2-\tau)}\mathrm{d}\tau]\,\phi_2\\
&\tau_{13} = (\tau_{13})_0\,\mathrm{e}^{-\frac{\mu}{\eta}t} + \tfrac{H(t_1)}{2\pi}\mu\,[U_1(t_1) - \tfrac{\mu}{\eta}\int_0^{t_1} U_1(\tau)\mathrm{e}^{-\frac{\mu}{\eta}(t_1-\tau)}\mathrm{d}\tau]\,\psi_3\\
&\qquad + \tfrac{H(t_2)}{2\pi}\mu\,[U_2(t_2) - \tfrac{\mu}{\eta}\int_0^{t_2} U_2(\tau)\mathrm{e}^{-\frac{\mu}{\eta}(t_2-\tau)}\mathrm{d}\tau]\,\phi_3\\
&\tau_{22} = \mathrm{e}^{-\frac{\mu}{\eta}t_2}(\tau_{22})_0\\
&\tau_{23} = \mathrm{e}^{-\frac{\mu}{\eta}t_2}(\tau_{23})_0\\
&\tau_{33} = \mathrm{e}^{-\frac{\mu}{\eta}t_2}(\tau_{33})_0\\
&e_{12} = (e_{12})_0 + \tfrac{\tau_\infty(0)}{2}[(\tfrac{1}{\eta} + \tfrac{k}{\mu})t + \tfrac{kt^2}{2\eta}] + \tfrac{U_1(t_1)}{4\pi}H(t_1)\psi_2 + \tfrac{U_2(t_2)}{4\pi}H(t_2)\phi_2\\
&e_{13} = (e_{13})_0 + \tfrac{U_1(t_1)}{4\pi}H(t_1)\psi_3 + \tfrac{U_2(t_2)}{4\pi}H(t_2)\phi_3
\end{aligned}\right\}. \tag{21}$$

Case-II:

If the fault F_1 is infinite strike-slip and the fault F_2 is finite dip-slip fault then for $t > T_2$ the slip condition can be characterized by:

$$\begin{aligned}
[u_3]_{F_2} &= U_3(t_2)\,f(y''_1,\ y''_3)\,H(t_2),\\
&\quad (-L \leqslant y''_1 \leqslant L,\ y''_2 = 0,\ 0 \leqslant y''_3 \leqslant D_2),\\
t_2 &\geqslant 0\,(t_2 = t - T_2)
\end{aligned} \tag{22}$$

where $[u_3]_{F_2}$ is the relative displacement across F_2 given by

$$[u_3]_{F_2} = \lim_{(y''_2 \to 0^+)}(u_3) - \lim_{(y''_2 \to 0^-)}(u_3) \tag{23}$$

$H(t_2)$ is the Heaviside function, $f(y''_1, y''_3)$ give the spatial dependence of the slip movement along the fault F_2 and $U_3(t_2) = v_2 t_2$, v_2 is the velocity of the F_2 fault movement.

Laplace transform of equation (22) gives

$[\bar{u_3}]_{F_2} = U_3(p)\,f(y''_1,\ y''_3)$, where $(\bar{u_3})$ is Laplace transform of u_3.

Now the displacement, stress and strain components for dip-slip movement of the fault F_2 are:

$$\left.\begin{aligned}
&(u_1)_3 = 0\\
&(u_2)_3 = 0\\
&(u_3)_3 = \tfrac{H(t_2)}{2\pi}U_3(t_2)\phi(z_1, z_2, z_3)\\
&(\tau_{11})_3 = 0\\
&(\tau_{12})_3 = 0\\
&(\tau_{13})_3 = 0\\
&(\tau_{23})_3 = \tfrac{H(t_2)}{2\pi}[U_3(t_2) - \tfrac{\mu}{\eta}\int_0^{t_2} U_3(\tau)\mathrm{e}^{-\frac{\mu}{\eta}(t_2-\tau)}\mathrm{d}\tau]\phi_2(z_1, z_2, z_3)\\
&(\tau_{22})_3 = 0\\
&(\tau_{33})_3 = \tfrac{H(t_2)}{2\pi}[U_3(t_2) - \tfrac{\mu}{\eta}\int_0^{t_2} U_3(\tau)\mathrm{e}^{-\frac{\mu}{\eta}(t_2-\tau)}\mathrm{d}\tau]\phi_3(z_1, z_2, z_3)\\
&(e_{12})_3 = 0\\
&(e_{13})_3 = \tfrac{H(t_2)}{4\pi}U_3(t_2)\phi_1(z_1, z_2, z_3)\\
&(e_{23})_3 = \tfrac{H(t_2)}{4\pi}U_3(t_2)\phi_2(z_1, z_2, z_3)\\
&(e_{33})_3 = \tfrac{H(t_2)}{4\pi}U_3(t_2)\phi_3(z_1, z_2, z_3)
\end{aligned}\right\}, \tag{24}$$

where ϕ given in appendix and $\phi_1 = \frac{\partial \phi}{\partial y_1}$, $\phi_2 = \frac{\partial \phi}{\partial y_2}$, $\phi_3 = \frac{\partial \phi}{\partial y_3}$.

The final solutions of displacement, stress and strain due to interaction between two faults, one infinite strike-slip and the other finite dip-slip fault are as follows:

$$
\left.
\begin{aligned}
u_1 &= (u_1)_0 + \tau_\infty(0)[(\tfrac{1}{\eta} + \tfrac{k}{\mu})t + \tfrac{kt^2}{2\eta}]y_2 + \tfrac{U_1(t_1)}{2\pi}\psi H(t_1)\\
u_2 &= 0\\
u_3 &= \tfrac{U_3(t_2)}{2\pi}H(t_2)\phi\\
\tau_{11} &= 0\\
\tau_{12} &= (\tau_{12})_0\, e^{-\frac{\mu}{\eta}t} + \tau_\infty(0)[1-e^{-\frac{\mu}{\eta}t} + kt] + \tfrac{H(t_1)}{2\pi}\mu\,[U_1(t_1)\\
&\quad -\tfrac{\mu}{\eta}\int_0^{t_1} U_1(\tau)e^{-\frac{\mu}{\eta}(t_1-\tau)}d\tau]\,\psi_2\\
\tau_{13} &= (\tau_{13})_0\, e^{-\frac{\mu}{\eta}t} + \tfrac{H(t_1)}{2\pi}\mu\,[U_1(t_1) - \tfrac{\mu}{\eta}\int_0^{t_1} U_1(\tau)e^{-\frac{\mu}{\eta}(t_1-\tau)}d\tau]\,\psi_3\\
\tau_{22} &= e^{-\frac{\mu}{\eta}t_2}(\tau_{22})_0\\
\tau_{23} &= \tfrac{H(t_2)}{2\pi}[U_3(t_2) - \tfrac{\mu}{\eta}\int_0^{t_2} U_3(\tau)e^{-\frac{\mu}{\eta}(t_2-\tau)}d\tau]\phi_2\\
\tau_{33} &= \tfrac{H(t_2)}{2\pi}[U_3(t_2) - \tfrac{\mu}{\eta}\int_0^{t_2} U_3(\tau)e^{-\frac{\mu}{\eta}(t_2-\tau)}d\tau]\phi_3\\
e_{12} &= (e_{12})_0 + \tfrac{\tau_\infty(0)}{2}[(\tfrac{1}{\eta} + \tfrac{k}{\mu})t + \tfrac{kt^2}{2\eta}] + \tfrac{U_1(t_1)}{4\pi}H(t_1)\psi_2\\
e_{13} &= (e_{13})_0 + H(t_1)\tfrac{\mu}{4\pi}\psi_3(y_2,\ y_3) + H(t_2)\tfrac{\mu}{4\pi}U_3(t_2)\phi_1\\
e_{23} &= \tfrac{H(t_2)}{4\pi}U_3(t_2)\phi_2\\
e_{33} &= \tfrac{H(t_2)}{4\pi}U_3(t_2)\phi_3
\end{aligned}
\right\} \quad (25)
$$

3.3. Numerical computations

It is to be noted that in both the models, fault F_1 is taken to be infinite while fault F_2 is taken to be finite.

We consider following numerical values of the model parameters as suggest Cathles (1975 [25]), Clift *et al* (2002 [26]) and Karato (2010 [27]):

$\mu = 3.5 \times 10^{10}$ N m^{-2}
$\eta = 3.5 \times 10^{19}$Pa s
$\tau_\infty(t) = 200$ bar $= 2 \times 10^7$ N m^{-2}
$t = 150$ year, $T_1 = 50$ year, $T_2 = 100$ years
$L = 10$ kms
$D_1 = 10$ km, $D_2 = 10$ km
$d_1 = 5$ km, $d_2 = 5$ km
$D = 8$ km
$v_1 = 1$ cm/year, $v_2 = 1$ cm/year
$\tau_\infty(t) = \tau_\infty(0)\ (1 + kt)$, $\quad k = 10^{-9}$
$\tau_\infty(0) = 20 \times 10^5$ N m^{-2}
$(\tau_{12})_0 = 20 \times 10^5$N m^{-2}
$(\tau_{13})_0 = 20 \times 10^5$ N m^{-2}.

For the inclinations θ_1 and θ_2 of the faults F_1 and F_2 respectively, we assume their values only in the range $0 \leqslant \theta_1 \leqslant \pi/2$ and $0 \leqslant \theta_2 \leqslant \pi/2$. For inclinations $\theta > \pi/2$, say $\theta = \pi - \theta_1(0 \leqslant \theta_1 \leqslant \pi/2)$ or $\theta = \pi - \theta_2(0 \leqslant \theta_2 \leqslant \pi/2)$, the nature of displacements, stresses and strains in the medium will be similar to the case for which θ_1 or $\theta_2 = \theta$. The values of θ_1 and θ_2 has been taken here as 30^0, 45^0, 60^0, 90^0 and creep function for infinite fault $f_1(y'_3) = U_1\left(1 - \frac{3y'^2_3}{D_1^2} + \frac{2y'^3_3}{D_1^3}\right)$ (Figure 2) and for finite fault $f_2(z'_1,\ z'_3) = U_2\ (1 - \frac{1}{L^2 z_1'^2})\left(1 - \frac{3}{D_2^2}z_3'^2 + \frac{3}{D_2^2}z_3'^3\right)$ (figure 3) where U_1, U_2 are constant and taken as $U_1 = 1$ cm and $U_2 = 1$ cm.

4. Result and discussion

(a) Rate of Change of surface displacement:

(i) Both F_1 and F_2 are strike-slip faults:

The rate of change of surface displacement R_{D_1} per year has been considered due to creeping movement only across F_1 ($T_1 < t < T_2$), there being no movement across F_2. This rate is given by $(R_{D_1}) = \frac{\partial}{\partial t}[u_1 - (u_1)_0 + \tau_\infty(0)\left[t\left(\frac{1}{\eta} + \frac{k}{\mu}\right) + \frac{kt^2}{2\eta}\right]y_2]$. In figure 4(a), R_{D_1} is plotted against y_2, the distance from the fault F_1 on free surface, including its limiting values as $y_2 \to 0^+$ and $y_2 \to 0^-$ for different inclinations of F_1. It is found that this rate depends significantly on the inclination θ_1 of the fault F_1. The maximum magnitude of the rate of change of surface displacement due to fault creep is attained near the fault for both $y_2 > 0$ and $y_2 < 0$. This rate decreases rapidly as we move away from the fault on either side of the free surface for all values of θ_1 but with varying rate. The rate of decrease of R_{D_1} with y_2 is higher for lower value of θ_1. This rate becomes very small for $y_2 \gg 0$. For $y_2 > 0$ and $y_2 < 0$ rates of change of surface displacement due to fault creep are of opposite sings. It is found that apart from these similarities, there are considerable differences between the rate of change of surface displacement due to fault creep for faults with different inclinations. For $y_2 > 0$, this rate is found to increase as θ_1 decreases. For $y_2 < 0$, this rate decreases as θ_1 increases. For $\theta_1 = 90^0$, the rate is anti-symmetrical with respect to $y_2 = 0$. However, for $\theta_1 \neq 90^0$, there is no such anti-symmetry.

In figure 4(b), R_{D_1} plotted against y_2 for different velocity of the fault movement across F_1 when there is no movement across F_2 and θ_1 is taken as 60^0. At $y_2 = 0$ i.e on the fault, rate of displacement is equal to zero. For $y_2 > 0$, it first increases rapidly and then decreases sharply towards zero for different velocities of F_1. For $y_2 < 0$, R_{D_1} first decreases rapidly and then increases gradually and finally tends towards zero. Rate of displacement attains its maximum and minimum value as $|y_2| \to 0$. For $y_2 > 0$, rate of displacement increases with increasing values of velocity and for $y_2 < 0$, it decreases with increasing values of velocity.

Figure 5 shows the rate of change of surface displacement (R_{D_1}) due to creeping movement across both F_1 and F_2 (for $t > t_2$) for different values of θ_1 and θ_2 and different values of v_1 and v_2. In figure 5 (a) and (b), rate of displacement has been plotted against y_2 for different inclination of the fault F_1 when inclination of F_2 is taken as 60^0 and 90^0 respectively. Comparing them with figure 4(a), it is found that there is no significant changes in the nature of R_{D_1} for $y_2 < 0$ after a movement across F_2. In this case for all θ_1, there is a change in R_{D_1} for $y_2 > 0$ only. A significant change is found in R_{D_1} in both the figure 5 (a) and (b) at a distance $D = 8$ km from F_1, where F_2 is located. It shows that when the fault F_2 starts creeping for $y_2 > D$, R_{D_1} is positive and increases

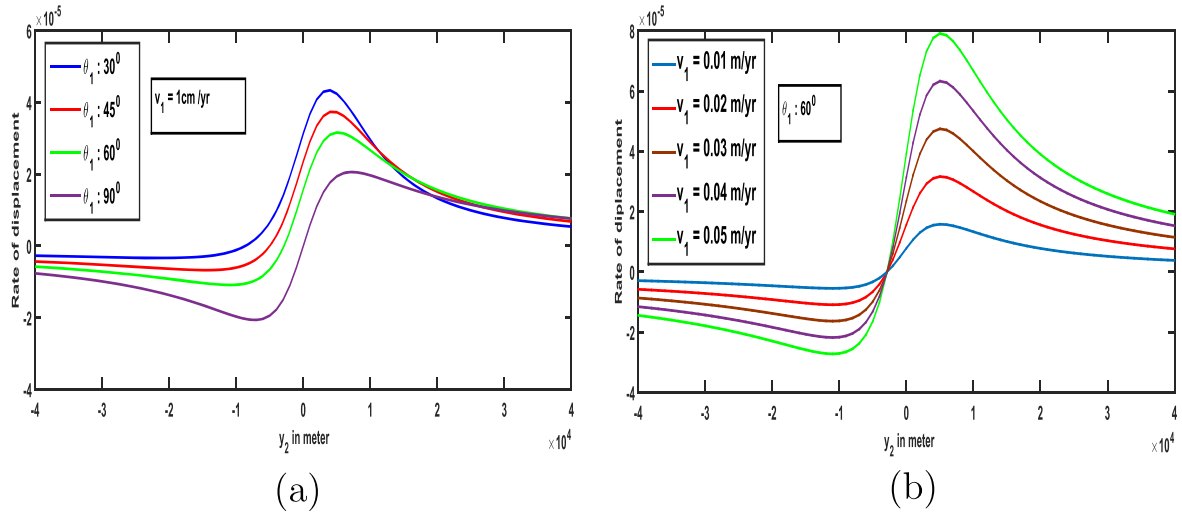

Figure 4. Rate of change of surface displacement with y_2 due to fault creep only across F_1 (no movement across F_2) (a) for different inclination of the fault and (b) for different velocity of the fault movement with $\theta_1 = 60^0$.

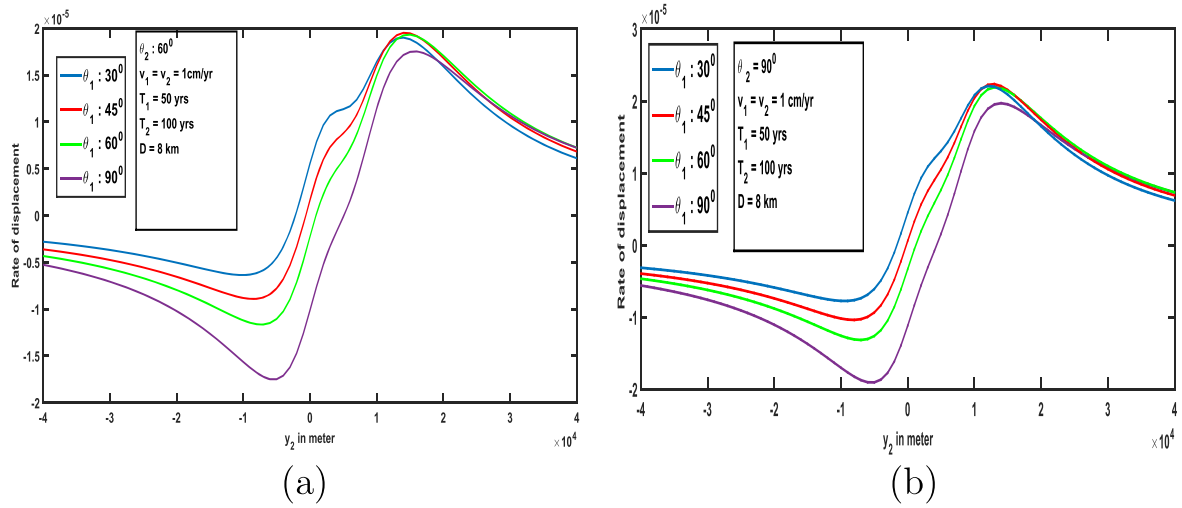

Figure 5. Rate of change of surface displacement with y_2 due to fault creep across both F_1 and F_2 for different inclination θ_1 of F_1 with (a) $\theta_2 = 60^0$ and (b) $\theta_2 = 90^0$.

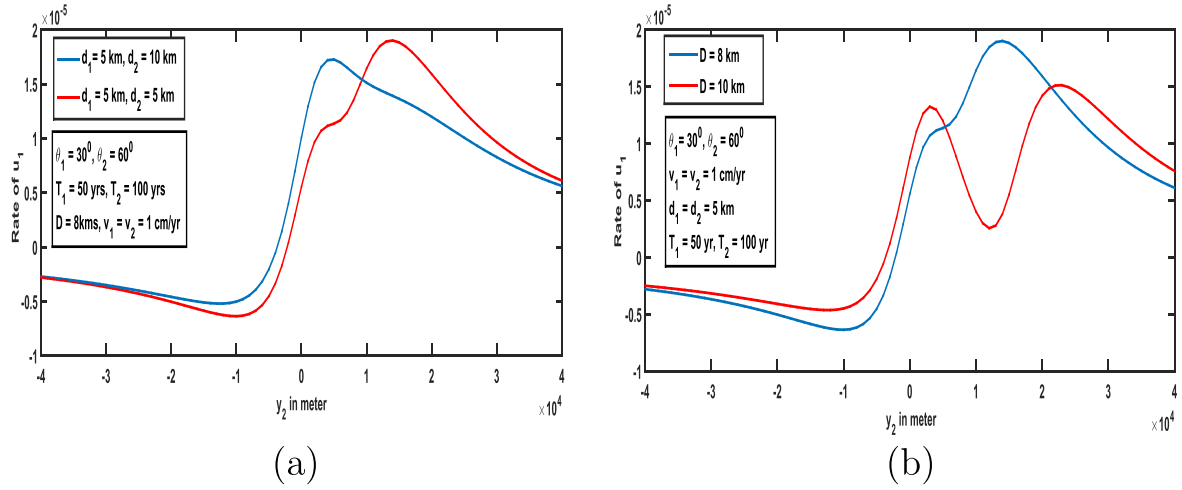

Figure 6. Rate of change of displacement (u_1) with y_2 after fault movement across F_1 and F_2 for (a) different depth of the fault from the free surface (b) different distance of the fault F_1 and F_2.

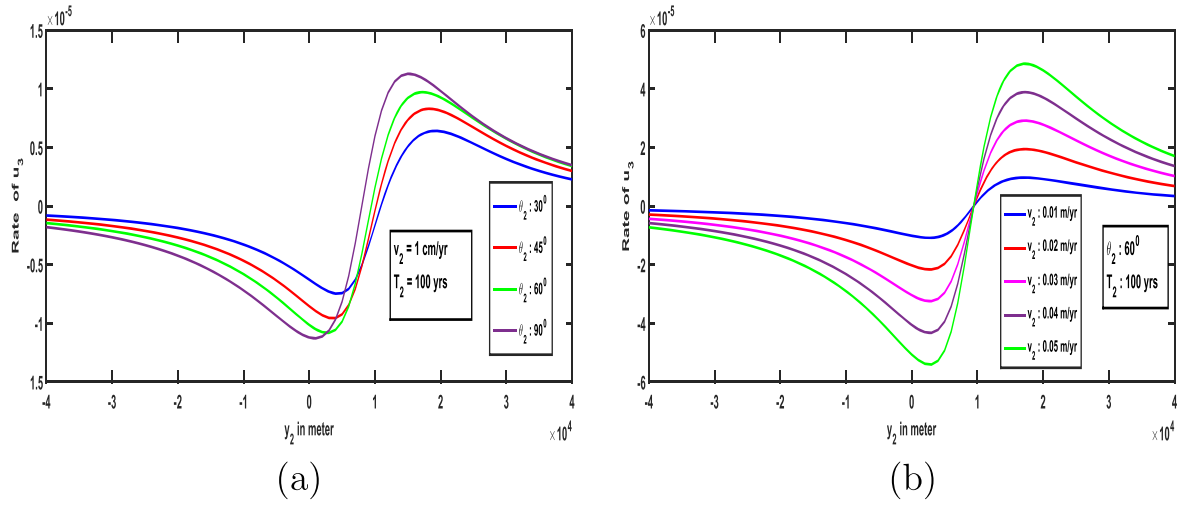

Figure 7. Rate of change of displacement (u_3) with y_2 after fault movement F_1 and F_2 for (a) different inclination θ_2 of F_2 (b) different velocity of the fault movement F_2.

sharply and then gradually decreases as y_2 become much greater than D. The maximum positive value of R_{D_1} for $y_2 > 0$ is attained near the fault F_2 and this value depends on θ_2. From figure 5 (a) and (b), it is observed that when $\theta_2 = 90^0$ rate of change of displacement for different inclination of θ_1 is greater than for $\theta_2 = 60^0$. If θ_1 and θ_2 are 90^0 that is both the faults are vertical then the fault displaced due to earthquake is less than the displacement of the other inclined faults which is clear from figure 5(b). The propagation of crack tips of the fault increases with displacement increases.

If the depth of the faults from the free surface increase then rate of displacement decrease which is described in figure 6 (a). If distance between two neighbouring fault is increasing then rate of u_1 is decreasing which is clear from figure 6 (b).

and the fault movement F_2 effects on displacement component u_3. That is if F_2 is dip-slip then rate of u_3 changes across the fault movement F_2 only. For F_1 infinite strike slip and F_2 finite dip-slip fault, there is a displacement of the fault F_1 in y_1 direction and F_2 in y_3 direction. The rate of change of displacement $R_{D_2} = \frac{\partial}{\partial t}(u_3) = \frac{\partial}{\partial t}\left[\frac{U_2(t_2)}{2\pi} H(t_2) e^{-\left(\frac{\mu}{\eta}\right)t}\phi\right]$ has been plotted against y_2 for different inclination of the fault F_2 and different velocity of the fault movement F_2 in figures 7 (a) and (b) respectively. It is observed that for $y_2 = 0$–8 km, the rate of change of displacement is very small while for $y_2 > 8$ km it is high.

(b) Rate of change of stress

(i) Both F_1 and F_2 are strike-slip fault:

The shear stresses $(T'_{12})_{F_1(\mathrm{MID})}$ and $(T''_{12})_{F_2(\mathrm{MID})}$ near the mid points of the faults F_1 and F_2 are respectively

$$\left.\begin{aligned}(T'_{12})_{F_1(\mathrm{MID})} &= \tau_{12}\sin\theta_1 - \tau_{13}\cos\theta_1 \\ &= (T'_{12})_{0F_1} e^{-\frac{\mu}{\eta}t} + \tau_\infty(0)\sin(\theta_1)[1 - e^{-\frac{\mu t}{\eta}} + kt] \\ &\quad + \frac{H(t-T_1)}{2\pi}\mu\left[U_1(t_1) - \frac{\mu}{\eta}\int_0^{t_1} U_1\tau e^{-\frac{\mu}{\eta}(t_1-\tau)}d\tau\right][\psi_2\sin\theta_1 - \psi_3\cos\theta_1] \\ &\quad + \frac{H(t-T_2)}{2\pi}\mu\left[U_2(t_2) - \frac{\mu}{\eta}\int_0^{t_2} U_2\tau e^{-\frac{\mu}{\eta}(t_2-\tau)}d\tau\right][\phi_2\sin\theta_1 - \phi_3\cos\theta_1]\end{aligned}\right\}, \tag{26}$$

(ii) F_1 is strike-slip and F_2 is dip-slip fault:

Since the fault F_1 is strike-slip and F_2 is finite dip-slip fault, then fault movement F_1 effects on displacement component u_1

where $(T'_{12})_{0F_1} = (\tau_{12})_0\sin\theta_1 - (\tau_{13})_0\cos\theta_1$ and

$$\left.\begin{aligned}(T''_{12})_{F_2(\mathrm{MID})} &= \tau_{12}\sin\theta_2 - \tau_{13}\cos\theta_2 \\ &= (T''_{12})_{0F_2} e^{-\frac{\mu}{\eta}t} + \tau_\infty(0)\sin(\theta_2)[1 - e^{-\frac{\mu t}{\eta}} + kt] \\ &\quad + \frac{H(t-T_1)}{2\pi}\mu\left[U_1(t_1) - \frac{\mu}{\eta}\int_0^{t_1} U_1\tau e^{-\frac{\mu}{\eta}(t_1-\tau)}d\tau\right][\psi_2\sin\theta_2 - \psi_3\cos\theta_2] \\ &\quad + \frac{H(t-T_2)}{2\pi}\mu\left[U_2(t_2) - \frac{\mu}{\eta}\int_0^{t_2} U_2\tau e^{-\frac{\mu}{\eta}(t_2-\tau)}d\tau\right][\phi_2\sin\theta_2 - \phi_3\cos\theta_2]\end{aligned}\right\}, \tag{27}$$

where $(T''_{12})_{0F_2} = (\tau_{12})_0\sin\theta_2 - (\tau_{13})_0\cos\theta_2$

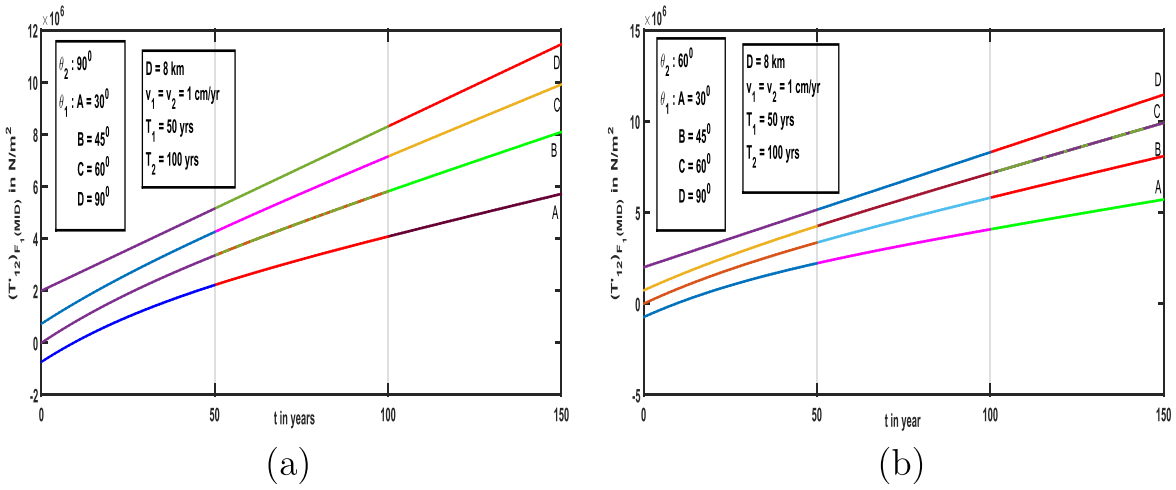

Figure 8. Total shear stress at the mid point of the fault F_1 for different values of θ_1 when (a) $\theta_2 = 90^0$ (b) $\theta_2 = 60^0$.

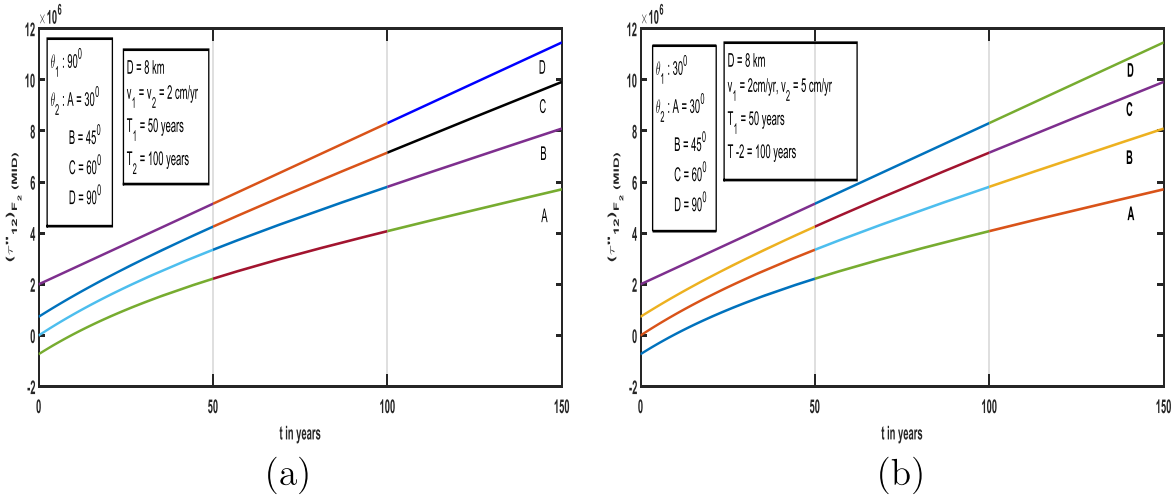

Figure 9. Total shear stress at the mid point of the fault F_2 for different values of θ_2 when (a) $\theta_1 = 90^0$ (b) $\theta_1 = 60^0$.

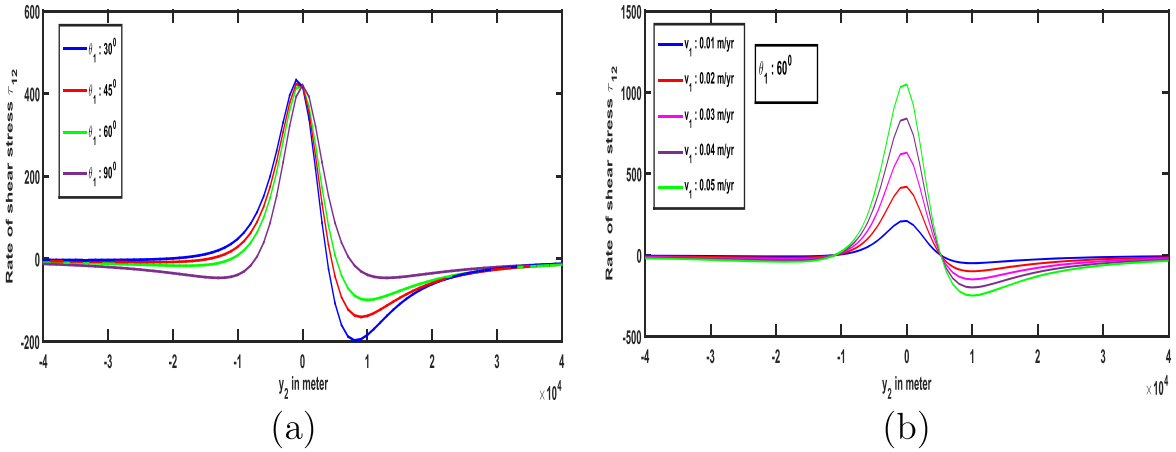

Figure 10. Rate of change of shear stress τ_{12} with y_2 due to fault creep across F_1 only (no movement across F_2) for (a) different inclination θ_1 of F_1 (b) different velocity of the fault movement.

We consider the shearing stresses $(T'_{12})_{F_1(\mathrm{MID})}$ and $(T''_{12})_{F_2(\mathrm{MID})}$ in the half-space which tends to cause movements across the faults. To study its changes with time the shearing stresses $(T'_{12})_{F_1(\mathrm{MID})}$ and $(T''_{12})_{F_2(\mathrm{MID})}$ have been plotted against time for moderate earthquake for different values of θ_1 and θ_2 in figures 8 and 9. These figures shows that the shearing stress $(T'_{12})_{F_1}$ near the fault F_1 gradually increases with time upto $t = T_1$ (=50 years), i.e. the instant at which F_1 starts creeping.

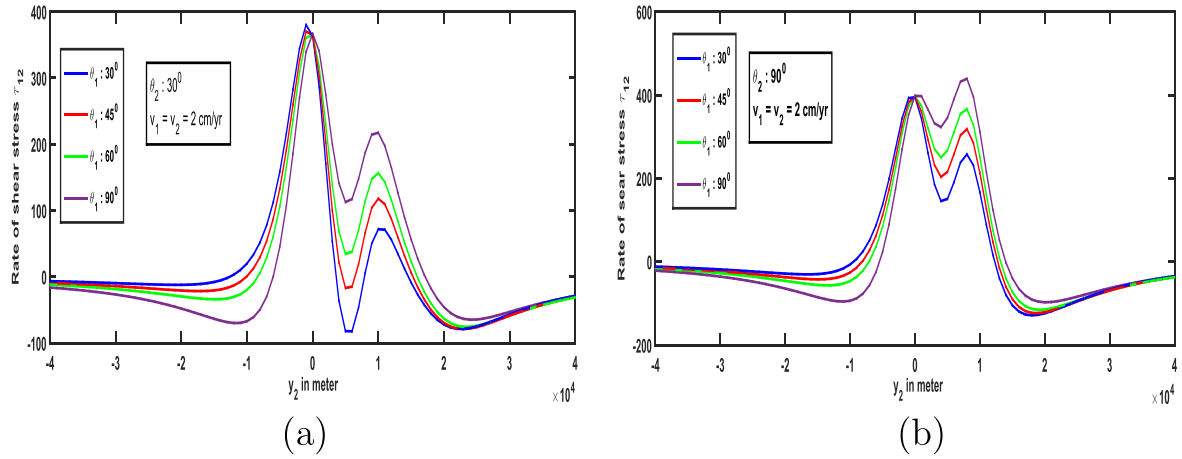

Figure 11. Rate of change of shear stress τ_{12} with y_2 due to fault creep across both F_1 and F_2 for different inclination θ_1 of F_1 with (a) $\theta_2 = 30^0$ and (b) $\theta_2 = 90^0$.

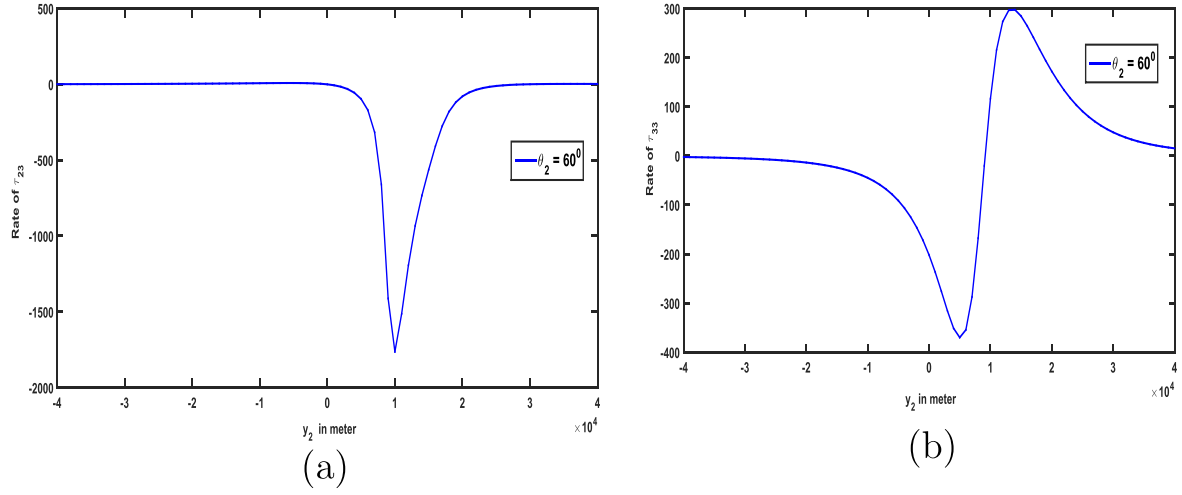

Figure 12. (a) Rate of change of stress τ_{23} with y_2 and (b) rate of change of stress τ_{33} with y_2.

At $t = T_1$, the slope of the curve changes. It continues upto $t = T_2$ (=100 years), i.e. the time when the fault F_2 starts creeping. After $t = T_2$, again there is a change of the slope of the shear stress curve. Figure 8 shows that the rate of increase of $(T'_{12})_{F_1(\mathrm{MID})}$ depends on θ_1, the inclination of the fault F_1 itself. For higher values of θ_1, the rate is higher, being maximum for $\theta_1 = 90^0$. This indicates the fact that there will be more accumulation of shearing stress near the vertical faults than the inclined faults with inclinations lesser than $\pi/2$.

Figure 9 shows the change of the shearing stress at the mid point of the fault F_2 denoted by $(\tau''_{12})_{F_2(\mathrm{MID})}$ with time. It is noted that in the absence of any fault movement, shear stress gradually accumulates in the system due to tectonic force τ_∞. The maximum limiting values that may be attained by $(T'_{12})_{F_1(\mathrm{MID})}$ near F_1 and $(T''_{12})_{F_2(\mathrm{MID})}$ near F_2 are $\tau_\infty \sin(\theta_1)$ and $\tau_\infty \sin(\theta_2)$ respectively. It is observed that in the absence of any fault movement ($t < T_1$), there is gradual accumulation of shear stress near F_1 with increasing rate of accumulation depending upon the inclination of the fault, being maximum for vertical faults. But after the commencement of fault creep across F_1 ($T_1 < t < T_2$), this rate of accumulation changes. This change depends on the inclination θ_1 and θ_2 with the horizontal. This pattern of stress accumulation near F_1 continues upto the instant $t = T_2$ at which second fault F_2 also starts creeping. At $t = T_1$ and $t = T_2$, there is a change in the rate of stress accumulation.

The rate of change of τ_{12} is $\frac{\partial}{\partial t}[\tau_{12} - (\tau_{12})_0, \mathrm{e}^{-\frac{\mu}{\eta}t} + \tau_\infty(0)$ $[1 - \mathrm{e}^{-\frac{\mu}{\eta}t} + kt]] = \frac{H(t-T_1)}{2\pi}\mu\,[U_1(t_1) - \frac{\mu}{\eta}\int_0^{t_1} U_1\tau \mathrm{e}^{-\frac{\mu}{\eta}(t_1-\tau)}\mathrm{d}\tau]$ $\psi_2 + \frac{H(t-T_2)}{2\pi}\mu\ [U_2(t_2) - \frac{\mu}{\eta}\int_0^{t_2} U_2\tau \mathrm{e}^{-\frac{\mu}{\eta}(t_2-\tau)}\mathrm{d}\tau]\ \phi_2$. Figure 10 has been explained the rate of chance of τ_{12} against y_2 for different inclinations and different velocities of the fault movement across F_1. The maximum stress is attained at $t = T_1$, i.e. when the fault F_1 starts creeping. Rate of stress accumulation/release of τ_{12} has been plotted against y_2 due to creeping movement of both the faults F_1 and F_2 in figure 11. It is seen that there is a significant change in τ_{12} at $D = 8$ km, i.e when the fault F_2 starts creeping. It is different for different inclination θ_1 of the fault F_1 when θ_2 is fixed. If θ_1 increases, rate of τ_{12} increases. From figures 11(a) and (b), it is analysed that the rate of change of τ_{12} depends on θ_2. This increases with increasing value of θ_2.

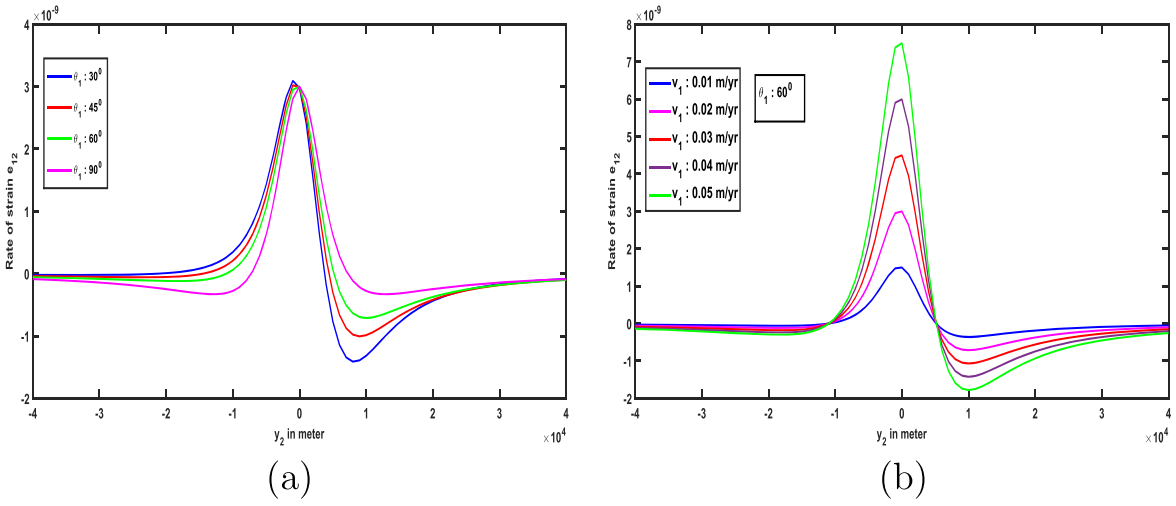

Figure 13. Rate of change of strain e_{12} with y_2 due to fault creep across F_1 only (no movement across F_2) for (a) different inclination θ_1 of F_1 and (b) different velocity v_1 of the fault movement.

(ii) F_1 infinite strike-slip fault and F_2 is finite dip-slip fault:

If F_1 is infinite strike-slip fault and F_2 is finite dip-slip fault then there is an effect on the stress component τ_{12} and τ_{13} after the fault movement across F_1 only. The fault movement across F_2 affects stress components τ_{23} and τ_{33}. The changes of rate of τ_{23} and τ_{33} with y_2 have been described in figures 12 and and (b) for $\theta_2 = 60^0$. It has been observed that after the fault movement across F_2 at $y_2 = 8$ km, τ_{23} (stress acting in the y_3 direction on the plane whose outward normal is parallel to the y_2 axis) decreases as y_2 increases and the maximum shear stress release occurs near $y_2 = 10$ km. After that it reaches zero near $y_2 = 20$ km. This indicates that maximum stress release occurs in the neighbourhood of the fault F_2 as seen in figure 12 (a). Figure 12(b) shows that for $y_2 > 0$, τ_{33} (normal stress along y_3 axis) decreases and attains minimum value near $y_2 = 8$ km, where F_2 is located. For $y_2 \geqslant 8$ km, it increases sharply and attains its maximum value near $y_2 = 10$ km followed by gradual decrease and it finally approaches to zero as y_2 increases further. That is for the stress component τ_{33}, normal stress along y_3 axis first releases and then accumulates.

(c) Rate of change of strain:

(i) Both F_1 and F_2 are strike-slip fault:

Now the nature of surface shear strain accumulation before and after the fault movement has been considered. The rate of change of surface shear strain $R_{S_1} = \frac{\partial}{\partial t}[e_{12} - (e_{12})_0 + \frac{\tau_\infty(0)}{2}\{t\left(\frac{1}{\eta} + \frac{k}{\mu}\right) + \frac{kt^2}{2\eta}\}] = [\frac{U_1(t_1)}{4\pi}H(t_1)\psi_2 + \frac{U_2(t_2)}{4\pi}H(t_2)\phi_2]$. It is noted that, in the absence of any fault movement, there is a steady accumulation of surface shear strain near the fault with time. After the commencement of a fault movement, this rate of strain accumulation falls off. The maximum reduction take place near the fault itself across which the movement occurs.

Figure 13 shows the rate of accumulation/release of shear strain per year near and away from the fault due to creep across F_1 ($y_2 \approx 0$, $y_3 = 0$), from $y_2 = -40$ km to $y_2 = +40$ km for different θ_1 and different velocity of fault movement. It is seen that the fault creep results in the accumulation/release of the surface shear strain and this effect decrease rapidly as we move far away from the fault trace on the free surface. For $\theta_1 = 90^0$, R_{S_1} is greatest near the fault trace ($y_2 \approx 0$, $y_3 = 0$) and is symmetrical about the fault trace. For $\theta_1 \neq 90^0$, the effect is not symmetrical. Maximum strain accumulates near the fault trace and maximum rate of release of surface shear strain occurs a little away from the fault trace. The rate of release of shear strain due to fault creep changes with change in the inclination θ_1 and velocity of the fault movement v_1. As θ_1 decreases from 90^0, rate of strain release increases more for $y_2 > 0$ and comparatively less for $y_2 < 0$. On the fault trace strain accumulation increases with velocity (v_1) of the fault movement across F_1. For $y_2 > 0$ and <0, rate of strain increase as velocity (v_1) increases. The differences in the effect of fault creep on the surface shear strain for different inclinations and velocity of the fault may be useful in estimating the inclinations and velocity of the creeping fault using observational data on aseismic change in the surface shear strain near the fault.

After the commencement of fault creep across F_2 the rate of shear strain changes significantly which is clear from figure 14. Near the fault F_1, R_{S_1} increases for all θ_1 and these increments in the values of R_{S_1} depend significantly on θ_2, higher the values of θ_2, higher the increments. As we move away from the fault F_1 and approaches towards F_2, R_{S_1} decreases first upto a certain level and then start increasing and reaches a higher value near F_2 and then it gradually decreases towards zero as $y_2 \gg D$. This value depends significantly on the inclination θ_2 of the fault F_2 but not so significantly on the inclination θ_1 of the fault F_1.

From figures 15 (a), (b) and 16, it is seen that if both the faults are infinite and both the faults are finite ([19]) then the rate of shear strain accumulation and release is different from that when F_1 is infinite and F_2 is finite. If we compare these

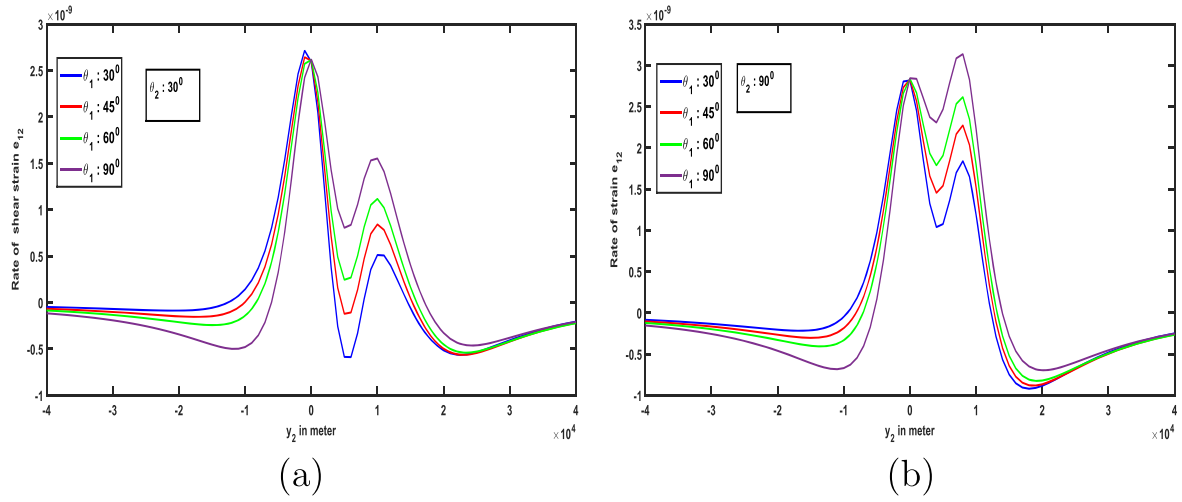

Figure 14. Rate of change of shear strain e_{12} with y_2 due to fault creep across both F_1 and F_2 for different inclination θ_1 of F_1 with (a) $\theta_2 = 30^0$ (b) $\theta_2 = 90^0$.

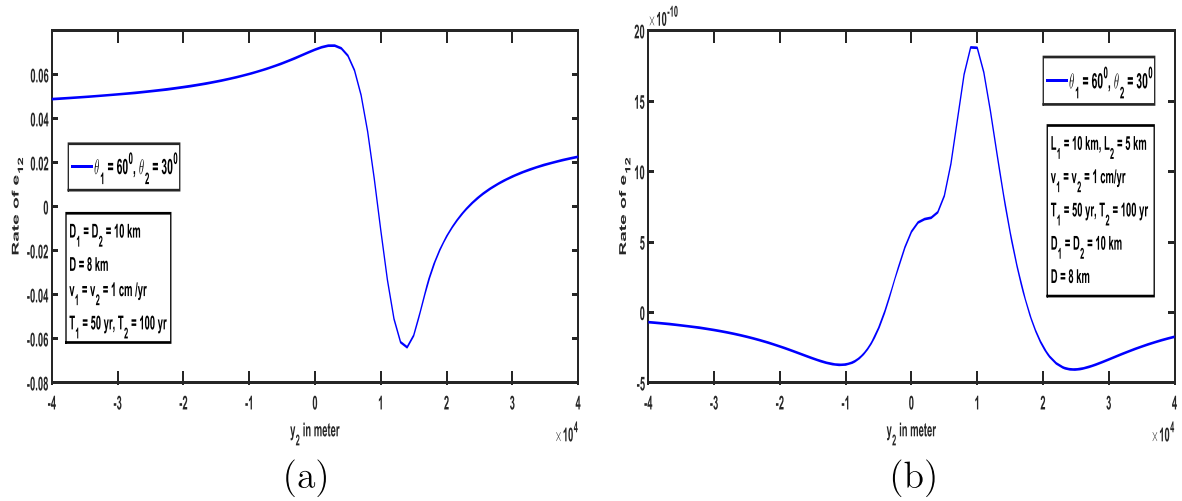

Figure 15. Rate of change e_{12} with y_2 after the fault movement across F_2 for (a) both the faults are infinite (b) both the faults are finite.

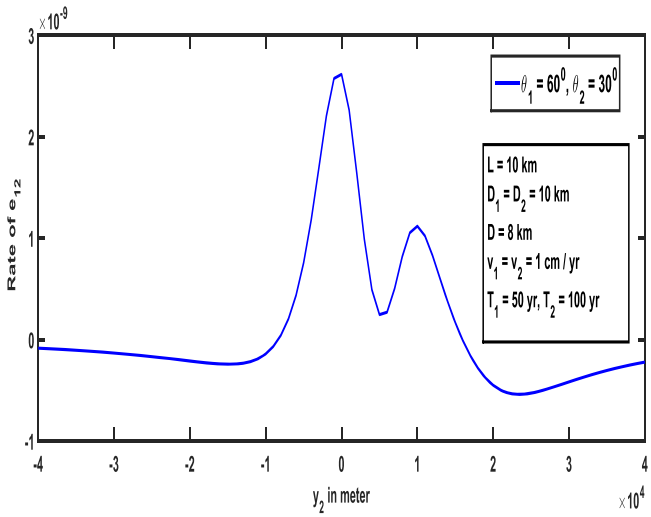

Figure 16. Rate of change e_{12} with y_2 after the fault movement across F_2 for F_1 infinite and F_2 finite.

three figures it is clear that rate of accumulation of shear strain is greater if both F_1, F_2 are infinite than that if F_1, F_2 finite as well as F_1 infinite, F_2 finite. It is also observed that rate of shear strain release is greater if both the faults are finite. The effect of fault movement of F_1 and F_2 on the rate of shear strain is more significant when F_1 is infinite and F_2 is finite (figure 16).

(ii) F_1 is long strike slip fault and F_2 is finite dip slip fault:

If the fault F_1 is infinite strike-slip and F_2 is finite dip-slip fault, then the movement across F_1 affects strain components e_{12} and e_{13} for t $\geqslant T_1$ and the movement across both F_1 and F_2 (t $\geqslant T_2$) affects the strain components e_{13}, e_{23} and e_{33}.

Rate of change of e_{23} (strain acting in the y_3 direction on the plane whose outward normal is parallel to the y_2 axis) is $\frac{\partial}{\partial t}(e_{23}) = \frac{\partial}{\partial t}[\frac{u_2(t_2)}{4\pi}H(t_2)\phi_2]$. Figure 17 shows that maximum strain e_{23} accumulates after the fault movement F_2 near y_2 $\approx$8 km. Rate of e_{23} with y_2 for different values of θ_2 has been plotted in figure 17(a). For $y_2 > 8$ km, rate of accumulation of

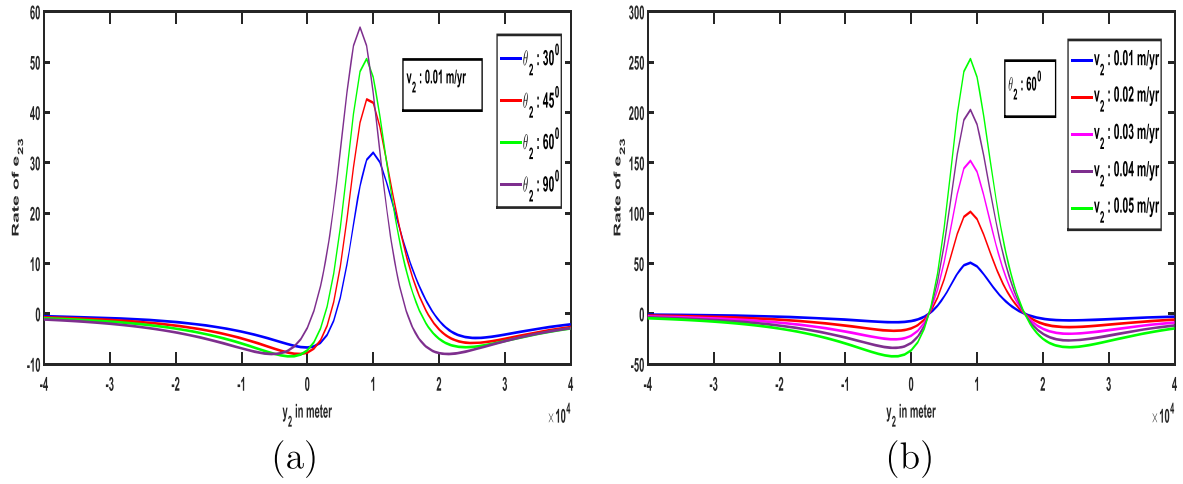

Figure 17. Rate of change e_{23} with y_2 after the fault movement across F_2 for (a) different inclination of the fault F_2 and (b) different velocity of the fault movement F_2.

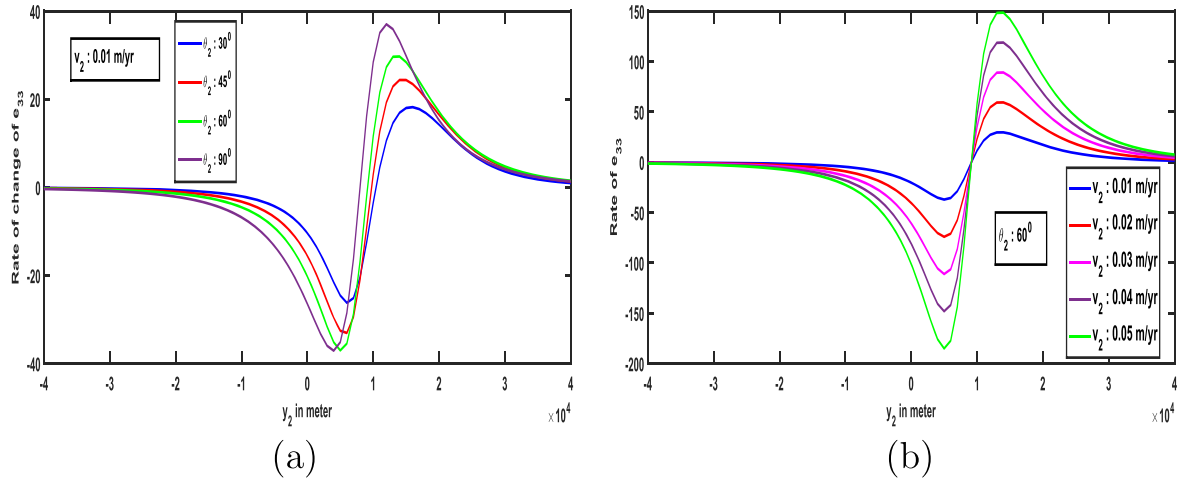

Figure 18. Rate of change of e_{33} with y_2 after the fault movement across F_2 for (a) different inclination of the fault F_2 and (b) different velocity of the fault movement F_2.

e_{23} is maximum and its value decreases as θ_2 decreases. Then it falls off rapidly and after releasing the strain it gradually increases and approaches towards zero. In figure 17(b), rate of e_{23} has been plotted against y_2 for different velocity of the fault movement F_2. If velocity decreases, strain accumulation decreases after the fault movement F_2.

The dip-slip nature of the fault F_2 affects the rate of change of e_{33} (normal strain along the y_3 axis). Rate of change of e_{33} is $\frac{\partial}{\partial t}(e_{33}) = \frac{\partial}{\partial t}\left[\frac{u_2(t_2)}{4\pi}H(t_2)\phi_3\right]$. Figure 18 shows that maximum strain e_{23} accumulates after the fault movement F_2 and then falls off rapidly towards zero. In figures 18(a) and (b), rate of change of e_{33} has been plotted against y_2 for different inclinations of the fault F_2 and for different velocity of the fault movement F_2.

From figures 17 and 18, It is seen that the maximum strain accumulates and releases near the fault F_2 and it is also true from practical view, since F_2 is dip-slip then the strain components e_{23} and e_{33} are affected by the fault movement F_2 only.

5. Conclusion

In the present model, two buried, inclined interacting faults—one infinite and the other finite—have been considered. A detailed study of deformation of the half-space due to creeping effect on displacement, stress and strain is analysed when (i) both the faults are strike-slip type and (ii) one strike-slip (infinite), other dip-slip (finite) type. If both the faults are strike-slip then they release their energy through rock displacement in a horizontal direction that is in y_1 direction in our model. On the other hand if one is strike-slip and the other dip-slip then the displacement will be both in horizontal and vertical direction that is in y_1 and y_3 direction of our model. For case (i) stress (components τ_{12}, τ_{13}) and strain (components e_{12}, e_{13}) accumulate and/or release and for case (ii) stress components τ_{12}, τ_{13}, τ_{23}, τ_{33} and strain components e_{12}, e_{13}, e_{23}, e_{33} have effect on the deformation due to earthquake fault. For infinite and finite interacting faults, the effect of interaction is more prominent than both infinite and both finite fault. The result emerges that an already existing

slip zone can activate the movement and slip along a neighbouring slip zone. In our interacting fault model, due to stress drop the local yield strength increases noticeably whereas for single fault (Cowie and Scholz (1992a)[28]) the stress concentration is same as the local yield strength at the tip of the fault. In order to enhancement of the length of the fault, interacting fault requires sufficient strain energy to break new fault surface ahead of the fault tip and to overcome the drop in shear stress that is obtained by a neighbouring fault. Consequently, as a fault grows toward another fault's stress drop region, its growth is retarded (figures 11(a) and (b)). Figures 5 and 11 show that the tip propagation is proportional to the rate of increase of displacement near the fault tip in the higher stress drop region. This observation suggests an expected sequence of displacement accumulation on interacting fault pairs. In this sequence, during advanced stages of interaction most displacement accumulates in the over-lap zone (figures 5(a) and (b)). This is supported by observations of a three-segment array from the Malawi Rift Basin, East Africa. It is also observed that the fault interaction at the slipping zone becomes stronger as the angle approaches towards 90^0 and the velocity increases.

Such study may throw some light to foretell about the occurrence of future fault movement and thereby help for making earthquake prediction program which may eventually save enormous life and property.

In future the concept of this paper can be extended for mediums (like Standard liner solid, Burger Rheology etc.) other than Maxwell type. It can also be extended for non-planer faults instead of plane faults as discussed in out model.

Compliance with ethical standards

Funding

The first author acknowledges DST-INSPIRE, INDIA for this financial assistance to carry out this study.

Conflict of Interest

The authors declare that they have no conflict of interest.

Appendix

To solve the boundary value problem, we assume that $\bar{u_1}$ has the form

$$\bar{u_1}(y_2,\ y_3,\ p) = \frac{(u_1)_0}{p} + B_1 y_2 + C_1 y_3. \tag{28}$$

Now taking Laplace transform on all constitutive equations and boundary conditions (from 3 to 10) we get

$$\bar{\tau_{12}} = \frac{\frac{1}{\mu}(\tau_{12})_0 + p\frac{\partial \bar{u_1}}{\partial y_2} - \left(\frac{\partial u_1}{\partial y_2}\right)_0}{\frac{1}{\eta} + \frac{p}{\mu}}, \tag{29}$$

$$\bar{\tau_{13}} = \frac{\frac{1}{\mu}(\tau_{13})_0 + p\frac{\partial \bar{u_1}}{\partial y_3} - \left(\frac{\partial u_1}{\partial y_3}\right)_0}{\frac{1}{\eta} + \frac{p}{\mu}}, \tag{30}$$

$$\left.\begin{aligned} \bar{\tau_{12}} &= \tau_\infty(0)\left(\frac{1}{p} + \frac{k}{p^2}\right) \\ \bar{\tau_{13}} &= 0 \end{aligned}\right\}. \tag{31}$$

Now putting the value from (25) in (29), (30) and using boundary conditions (31) and initial conditions we get the values of B_1 and C_1. Then substituting the value of B_1 and C_1 in equation (25) and taking inverse Laplace transform we get

$$(u_1)_1 = (u_1)_0 + \tau_\infty(0)\left[t\left(\frac{1}{\eta} + \frac{k}{\mu}\right) + \frac{kt^2}{2\eta}\right].$$

Since the fault F_1 is strike slip and infinite so $(u_2)_1 = 0$ and $(u_3)_1 = 0$.

We also get

$$\left.\begin{aligned} (\tau_{11})_1 &= 0 \\ (\tau_{12})_1 &= (\tau_{12})_0 e^{-\frac{\mu}{\eta}t} + \tau_\infty(0)[1 - e^{-\frac{\mu}{\eta}t} + kt] \\ (\tau_{13})_1 &= (\tau_{13})_0 e^{-\frac{\mu}{\eta}t} \\ (\tau_{22})_1 &= 0 \\ (\tau_{23})_1 &= 0 \\ (\tau_{23})_1 &= 0 \\ (e_{12})_1 &= (e_{12})_0 + \frac{\tau_\infty(0)}{2}\left[t\left(\frac{1}{\eta} + \frac{k}{\mu}\right) + \frac{kt^2}{2\eta}\right] \end{aligned}\right\}. \tag{32}$$

Differentiating the first and second equation of (3) w.r.t y_2 and y_3 we get

$$\frac{1}{\eta}\frac{\partial}{\partial y_2}\tau_{12} + \frac{1}{\mu}\frac{\partial^2}{\partial t \partial y_2}\tau_{12} = \frac{1}{2}\left(\frac{\partial^2 u_1}{\partial y_2^2} + \frac{\partial^2 u_2}{\partial y_1 \partial y_2}\right), \tag{33}$$

$$\frac{1}{\eta}\frac{\partial}{\partial y_3}\tau_{13} + \frac{1}{\mu}\frac{\partial^2}{\partial t \partial y_3}\tau_{13} = \frac{1}{2}\left(\frac{\partial^2 u_1}{\partial y_3^2} + \frac{\partial^2 u_3}{\partial y_1 \partial y_3}\right). \tag{34}$$

Now adding equation (33) and (34) and using (5) we get, $\frac{1}{\eta}\left(\frac{\partial}{\partial y_2}\tau_{12} + \frac{\partial}{\partial y_3}\tau_{13}\right) + \frac{1}{\mu}\frac{\partial}{\partial t}\left(\frac{\partial}{\partial y_2}\tau_{12} + \frac{\partial}{\partial y_3}\tau_{13}\right) = \frac{1}{2}\left(\frac{\partial^2 u_1}{\partial y_2{}^2} + \frac{\partial^2 u_1}{\partial y_3{}^2}\right) + \frac{1}{2}\frac{\partial}{\partial y_1}\left(\frac{\partial u_2}{\partial y_2} + \frac{\partial u_3}{\partial y_3}\right)\frac{1}{2}\left(\frac{\partial^2 u_1}{\partial y_2{}^2} + \frac{\partial^2 u_1}{\partial y_3{}^2}\right) + \frac{1}{2}\frac{\partial}{\partial y_1}\left(\frac{\partial u_2}{\partial y_2} + \frac{\partial u_3}{\partial y_3}\right) = 0.$

Since for infinite strike-slip fault displacement components are independent of y_1 then $\frac{1}{2}\left(\frac{\partial^2 u_1}{\partial {y_2}^2} + \frac{\partial^2 u_1}{\partial {y_3}^2}\right) = 0$. This can be written as $\frac{1}{2}\left(\frac{\partial^2 u_1}{\partial {y_1}^2} + \frac{\partial^2 u_1}{\partial {y_2}^2} + \frac{\partial^2 u_1}{\partial {y_3}^2}\right) = 0$. So

$$\nabla^2(u_1) = 0. \tag{35}$$

Now we take $G'_{13} = \frac{1}{2\pi}\left[\frac{y_3 - \xi_3}{L^2} - \frac{y_3 + \xi_3}{M^2}\right]$ and $G'_{12} = \frac{1}{2\pi}\left[\frac{y_2 - \xi_2}{L^2} + \frac{y_2 - \xi_2}{M^2}\right]$ where $L^2 = (y_2 - \xi_2)^2 + (y_3 - \xi_3)^2$ and $M^2 = (y_2 - \xi_2)^2 + (y_3 + \xi_3)^2$ $(\bar{u_1})_2(Q_1) = \frac{U_1(\bar{p})}{2\pi}\psi(y_2,\ y_3)$.

Taking inverse Laplace transform we get, $(u_1)_2 = \frac{U_1(t_1)}{2\pi}H(t - T_1)\psi(y_2,\ y_3)$ where

$$\psi = \int_0^{D_1} f(\xi'_3)\left[\frac{(y_2\sin\theta_1 - y_3\cos\theta_1) + d_1\cos\theta_1}{{\xi'_3}^2 - 2\xi'_3(y_2\cos\theta_1 + y_3\sin\theta_1) + ({y_2}^2 + {y_3}^2) + d_1^2 - 2y_3d_1 - 2d_1\xi'_3\sin\theta_1}\right.$$
$$\left. + \frac{(y_2\sin\theta_1 + y_3\cos\theta_1) + d_1\cos\theta_1}{{\xi'_3}^2 - 2\xi'_3(y_2\cos\theta_1 - y_3\sin\theta_1) + ({y_2}^2 + {y_3}^2) + d_1^2 + 2y_3d_1 + 2d_1\xi'_3\sin\theta_1}\right]\mathrm{d}\xi'_3.$$

The resulting boundary value problem can be now stated as $(u_1)_2$ satisfy $\nabla^2(\bar{u_1})_2 = 0$, where $(\bar{u_1})_2$ is the Laplace transform of $(u_1)_2$ w.r.t t with modified boundary conditions.

To solve this boundary value problem, a suitable modified form of Greens function technique developed by Maruyamma (1966 [22]) and Rybicki (1971 [23]). Following Maruyamma (1966 [22])

$$(\bar{u_1})_2(Q_1) = \int_{F_1}[(\bar{u_1})_2(p)]\quad [G'_{13}(Q_1,\ P_1)\mathrm{d}\xi_2 - G'_{12}(Q_1,\ P_1)\,\mathrm{d}\xi_3], \tag{36}$$

where $Q_1(y_1,\ y_2,\ y_3)$ is the field point in the half-space and $P_1(\xi_1,\ \xi_2,\ \xi_3)$ is any point on the fault F_1 . $0 \leqslant \xi_2 \leqslant D\cos\theta_1$, $0 \leqslant \xi_3 \leqslant D\sin\theta_1$, and $\xi_2 = \xi_3\cot\theta_1$.

A change in co-ordinate axes from $(\xi_1,\ \xi_2,\ \xi_3)$ to $(\xi_1,\ \xi'_2,\ \xi'_3)$ connected by the relation

$$\left.\begin{aligned}\xi_1 &= \xi'_1\\ \xi_2 &= \xi'_2\sin\theta_1 + \xi'_3\cos\theta_1\\ \xi_= &- \xi'_c os\theta_1 + \xi'_3\sin\theta_1 + d_1\end{aligned}\right\}. \tag{37}$$

From $\xi_2 = \xi_3\cot\theta_1$ we get, $\xi'_2 = 0$.

Then from equation (37) $\xi_1 = \xi'_1$, $\xi_2 = \xi'_3\cos\theta_1$ and $\xi_3 = \xi'_3\sin\theta_1 + d_1$

So, $\mathrm{d}\xi_1 = \mathrm{d}\xi'_1$ and $\mathrm{d}\xi_3 = \sin\theta_1\mathrm{d}\xi'_3$.

Now $(\bar{\tau_{12}})_2 = \frac{p}{\frac{1}{\eta} + \frac{p}{\mu}}\frac{\partial}{\partial y_2}(\bar{u_1})_2 = \frac{p}{\frac{1}{\eta} + \frac{p}{\mu}}\frac{U_1(p)}{2\pi}\psi_2$ where $\psi_2 = \frac{\partial\psi}{\partial y_2}$.

Taking inverse Laplace transform w.r.t t_1 and noting that $(\bar{\tau_{12}})_2 = 0$ for $t_1 \leqslant 0$

$$(\tau_{12})_2 = H(t - T_1)\frac{\mu}{2\pi}[U_1(t_1) - \frac{\mu}{\eta}\int_0^{t_1} U_1(t_1)\mathrm{e}^{-\frac{\mu}{\eta}(t_1-\tau)}\mathrm{d}\tau]\psi_2.$$

Similarly $(\tau_{13})_2 = H(t - T_1)\frac{\mu}{2\pi}[U_1(t_1) - \frac{\mu}{\eta}\int_0^{t_1} U_1(t_1)\mathrm{e}^{-\frac{\mu}{\eta}(t_1-\tau)}\mathrm{d}\tau]\psi_3$ where $\psi_3 = \frac{\partial\psi}{\partial y_3}$

and $(e_{12})_2 = H(t - T_1)\frac{U_1(t_1)}{4\pi}\psi_2$.

In similar way we can compute $(u_1)_3$ due to sudden movement of the fault F_2 where $(z_1,\ z_2,\ z_3)$ is the field point in the half space and $(\xi''_1,\ \xi''_2,\ \xi''_3)$ is the fault point. By simple linear transformation of co-ordinate $(z_1,\ z_2,\ z_3)$ and $(\xi''_1,\ \xi''_2,\ \xi''_3)$ to $(y''_1,\ y''_2,\ y''_3)$ and $(\eta'_1,\ \eta'_2,\ \eta'_3)$.

Then $(u_1)_3 = \frac{U_2(t_2)}{2\pi}H(t - T_2)\phi(y_1,\ y_2,\ y_3)$ where

$$\phi = \int_{-L}^{L}\int_0^{D_2} f_2(\eta'_1,\ \eta'_3) \times\left[\frac{z_2 - \xi'_2}{\{(z_1 - \xi'_1)^2 + (z_2 - \xi'_2)^2 + (z_3 - \xi'_3)^2\}^{\frac{3}{2}}}\right.$$
$$\left. + \frac{z_2 - \xi'_2}{\{(z_1 + \xi'_1)^2 + (z_2 - \xi'_2)^2 + (z_3 - \xi'_3)^2\}^{\frac{3}{2}}}\right]\sin\theta_2\mathrm{d}\eta'_1\ \mathrm{d}\eta'_3$$

$z_2 = y_2 - D$ and $z_3 = y_3 - d_2$.

Now by co-ordinate transform we get, $\xi'_1 = \eta'_1$

$\xi'_2 = \eta'_2\sin\theta_2 + \eta'_3\cos\theta_2$,

$\xi'_3 = -\eta'_2\cos\theta_2 + \eta'_3\sin\theta_2$.

Since $\eta'_2 = 0$, $0 \leqslant \eta'_3 \leqslant D_2$ on F_2

Then $\xi'_1 = \eta'_1$

$\xi'_2 = \eta'_3\cos\theta_2$,

$\xi'_3 = \eta'_3\sin\theta_2$.

References

[1] Mukhopadhyay A, Sen S and Maji P 1978b On the interaction between two locked strike-slip faults *Proc. Sixth Int. Symp. on Earthquake Engineering Roorkee* 1, pp 77–82 https://scholar.google.com/scholar?hl=en&as_sdt=0%2C5&q=On+the+interaction+between+two+locked+strike-slip+faults&btnG=

[2] Maji M, Sen S, Pal B P and Mukhopadhyay A 1979c On stress accumulation in the lithosphere and interaction between two strike-slip faults Indian *J. Meteol. Hudrol. Geophys. (Mausam)* **30** 359–63 https://metnet.imd.gov.in/mausamdocs/130234_F.pdf

[3] Mukhopadhyay A and Mukherji P 1984 On two interacting creeping vertical surface breaking strike-slip faults in the lithosphere Bull *ISET* **21** 163–91 https://scholar.google.com/scholar?hl=en&as_sdt=0%2C5&q=On+two+interacting+creeping+vertical+surface+breaking+strike-slip+faults+in+the+lithosphere&btnG=

[4] Mukhopadhyay A and Mukherji P 1986 On two aseismically creeping and interacting buried vertical strike-slip faults in the lithosphere *Bull., ISET* **23** 91–117 http://pascal-francis.inist.fr/vibad/index.php?action=getRecordDetail&idt=8371827

[5] Ghosh U, Mukhopadhyay A and Sen S 1992a On two aseismic creeping and interacting vertical strike-slip faults- one buried and the other extended up to the surface in a two layer model of the lithosphere *Bull. Ind. Sos. Earth Tech.* **29** 1–15 http://pascal-francis.inist.fr/vibad/index.php?action=getRecordDetail&idt=4333737

[6] Ghosh U, Mukhopadhyay A and Sen S 1992b On two interacting creeping vertical surface breaking strike-slip faults in a two layer model of the lithosphere *Phys. Earth Planet. Inter.* **70** 119–29

[7] Ghosh U and Sen S 2011 Stress accumulation near buried faults in the lithosphere-asthenosphere system *Int. J. Comput.* **1** 786–95 https://www.scirp.org/(S(i43dyn45teexjx455qlt3d2q))/reference/ReferencesPapers.aspx?ReferenceID=801811

[8] Kato N and Lei X 2001 Interaction of parallel strike-slip faults and a characteristic distance in the spatial distribution of active faults *Geophys. J. Int.* **144** 157–64

[9] Bonafede M, Boschi E and Dragoni M 2007 A dislocation model of microplate boundary ruptures in the presence of a viscoelastic asthenosphere *Geophys. J. Int.* **76** 515–29

[10] Debnath P and Sen S 2014 Two Neighbouring Strike Slip Fault and Their Interaction IOSR *J. Appl. Geol. Geophys.* **2** 44–56

[11] Wesnousky S G 1988 Seismological and structural evolution of strike-slip faults *Nature* **335** 340–3

[12] Parsons T, Sliter R, Geist E L, Jachens R C, Jaffe B E, Foxgrover A, Hart P E and McCarthy J 2003 Structure and mechanics of the hayward-rodgers creek fault step-over, San Francisco Bay, California *Bull. Seismol. Soc. Am.* **93** 2187–200

[13] Oglesby D D 2005 The dynamics of strike-slip step overs with linking dip-slip faults *Bull. Seismol. Soc. Am.* **95** 1604–22

[14] Harris R A and Day S M 1993 Dynamics of fault interaction: parallel strike-slip faults *J. Geophys. Res.* **98** 4461–72

[15] Segall P and Pollard D D 1980 Mechanics of discontinuous faults *J. Geophys. Res.* **83** 4337–50

[16] Mavko G M 1982 Fault interaction near hollister, California *J. Geophys. Res.* **87** 7807–16

[17] Shao B and Guiting H 2019 The interactions of fault patterns and stress fields during active faulting in central north China Block: Insights from numerical simulations *Chin. Acad. Geol. Sci.* **14** e0215893

[18] Attanayake J, Sandiford D, Schleicher L S, Jones A, Gibson G and Sandiford M 2019 Interacting intraplate fault systems in australia: the 2012 thorpdale, victoria, seismic sequences *J. Geophys. Res.: Solid Earth* **124** 4673–93

[19] Debnath S K 2013 Two interacting creeping vertical rectangular strike-slip faults in a viscoelastic half-space model of the lithosphere *Int. J. Sci. Eng. Res.* **4** 1058–71 https://pdfs.semanticscholar.org/b467/86ba6b8f8f8669a7937a093a21ed091e667f.pdf?_ga=2.78516628.1638182796.1580322474-559482601.1580322474

[20] Manna K and Sen S 2017 Interacting inclined strike-slip faults in a layered medium *Mausam* **68** 487–98 https://metnet.imd.gov.in/mausamdocs/16838_F.pdf

[21] Maruyama T 1964 Statical elastic dislocations in an infinite and semi-infinite medium Bull *Earthq. Res. Inst.* **42** 289–368 https://scholar.google.com/scholar?hl=en&as_sdt=0%2C5&q=Statical+elastic+dislocations+in+an+infinite+and+semi-infinite+medium&btnG=

[22] Maruyama T 1966 On two dimensional dislocations in an infinite and semi-infinite medium Bull *Earthq. Res. Inst.* **44** 811–71 https://scholar.google.com/scholar?hl=en&as_sdt=0%2C5&q=On+two+dimensional+dislocations+in+an+infinite+and+semi-infinite+medium+Bull.+Earthquake&btnG=

[23] Rybicki K 1971 The elastic residual field of a very long strike-slip fault in the presence of a discontinuity bull *Seis. Soc. Am.* **61** 79–92 https://pubs.geoscienceworld.org/ssa/bssa/article-abstract/61/1/79/116912/The-elastic-residual-field-of-a-very-long-strike?redirectedFrom=fulltext

[24] Rybicki K 1973 Static deformation of a multilayered half-space by a very long strike-slip fault *Pure Appl. Geophys.* **110** 1955–66

[25] Cathles L M III 1975 *The Viscoelasticity of the Earth's Mantle* (Princeton N. J: Princeton University Press) https://press.princeton.edu/books/hardcover/9780691644929/viscosity-of-the-earths-mantle

[26] Clift P, Lin J and Baarckhausen U 2002 Evidence of low flexural rigidity and low viscosity lower continental crust during continental break—up in the South China *Mar. Pet. Geol.* **19** 951–70

[27] Karato S 2010 Rheology of the Earth's mantle A historical review *Gondwana Res.* **18** 17–45

[28] Cowie P A and Scholz C H 1992a Physical explanation for the displacement-length relationship of faults using a post-yield fracture mechanics model *J. Struct. Geol.* **14** 1133–48